08,10,13

The effect of a nanocrystal size and shape on the baric and temperature dependences of its properties (Review)

© M.N. Magomedov

Institute for geothermal problems and renewable energy —
branch of the joint Institute of high temperatures of the Russian Academy of Sciences,
Makhachkala, Russia

E-mail: mahmag4@mail.ru

Received June 6, 2024
Revised July 5, 2024
Accepted August 4, 2024

The problems of studying the lattice properties of a nanocrystal at various pressures and temperatures are discussed. The changes in the equation of state and baric dependences of various properties of gold during the transition from macro- to nanocrystal of cubic or rod-like shape of 306 atoms were analyzed. The following properties were considered: Debye temperature, first and second Grüneisen parameters, elastic modulus, thermal expansion coefficient, isochoric and isobaric heat capacity, specific free surface energy and its derivative by temperature, melting point. The pressure derivatives of these functions were also considered. The presented dependences are compared with the results of other authors and the problems of calculation of these properties by different methods are discussed. It was shown that at isomorphic-isothermo-isobaric reduction of a nanocrystal size the values of some properties decrease, others — increase, and there are some that can change their size dependence at change of $P-T$-conditions. It was shown that when the nanocrystal shape deviates from the energy-optimal shape, the size changes of the baric dependences are increase.

Keywords: nanocrystal, surface energy, equation of state, thermal expansion, elastic modulus, melting point, gold.

DOI: 10.61011/PSS.2024.10.59615.151

Content

1. Introduction

In recent years, it was experimentally shown that size effects have a significant impact on the baric dependences of various properties of nanocrystals [1–3]. Meanwhile, changes in baric dependences with decreasing nanocrystal size have been studied relatively little theoretically, both analytically and using computer simulation. This is associated with that different calculation methods for properties of nanocrystal of N atoms include the specific (per unit area) surface free energy: σ, its size dependence at different pressures is difficult for determination.

The experimental measurement of σ value for the macrocrystal is remarkably laborious and is fimplemented only at atmospheric pressure and high temperatures [4–6]. At that, even at high temperatures, the accuracy of σ measurement is very low. As for the nanocrystals, the experimental dependence of σ function on nanocrystal size is as not reported yet, since the surface properties of the nanocrystals are hard to measure. That's why, in spite of many papers relating the calculation methods of function $\sigma(N)$, till now there is no clear and unambiguous answer to the question: whether the function $\sigma(N)$ decreases or increases during isomorphic (i.e. with unchanged shape) decrease in number of atoms in nanocrystal under constant pressure P and temperature T. Current literature (see, for example, Refs.[7–10]) comprises theoretical papers arguing both or decrease (this is reported primarily in analytical studies) and increase (this was determined via computer modeling) of function $\sigma(N)$ with an isomorphic-isothermal reduction in the size of the nanoparticle.

Thus, currently the dependence of function σ on temperature, specific (per atom) volume ($v = V/N$), size (or number of atoms) and shape of nanocrystal surface is difficult for description both analytically, and using computer simulation. However, without the dependence $\sigma(T, v, N)$ it is impossible to obtain the equation of state

of the nanocrystal, i.e. function $P(T, v, N)$. That is why it was not yet possible to theoretically study the baric dependences of properties of nanocrystals with its size isomorphic decreasing along various isotherms.

In our papers we suggested the analytical method (i.e. without computer simulation), ensuring calculation, based on pair potential of interatomic interaction, of both function $\sigma(T, v, N)$, and nanocrystal equation of state $P(T, v, N)$. Here we summarize results obtained by our method and specify the results obtained by other methods. At that, if in papers of other authors one or another method was developed to calculate the size dependences of specific properties only at $P = 0$, then here we demonstrate how under single method we can calculate the size changes of baric dependences of all lattice properties along various isotherms. Besides, under the same calculation method for the first time the derivatives of these dependences with respect to pressure, both during isomorphic change of size, and during isomeric (i.e. at constant N) change of nanocrystal shape.

2. Method for calculating the properties of macro- and nanocrystals

To calculate the lattice properties of the nanocrystal, it is necessary to determine both the interaction potential of its atom pair and the calculation method based on this potential. Such method was described in detail by us in Refs. [10,11]. Here we provide basic formulas to calculate the nanocrystal properties.

The pair interatomic interaction is represented by the Mie–Lennard-Jones potential in the form:

$$\phi(r) = \frac{D}{(b-a)}\left[a\left(\frac{r_o}{r}\right)^b - b\left(\frac{r_o}{r}\right)^a\right], \qquad (1)$$

where D and r_o are the depth and the coordinate of the potential minimum, $b > a > 1$ are numerical parameters, and r is the distance between atom centers.

Then, using the „only nearest neighbor interaction“approximation, the Debye temperature as a function of the first coordination number and the nanocrystal density can be determined as follows [12]:

$$\Theta(k_n, R) = A_w(k_n, R)\xi\left[-1 + \left(1 + \frac{8D}{k_B A_w(k_n, R)\xi^2}\right)^{1/2}\right]. \qquad (2)$$

Here, k_B is Boltzmann constant, k_n is first coordination number that in the nanocrystal depends on both its size and shape of its surface [13,14], $R = r_o/c$ is relative linear density, $c = (6k_p v/\pi)^{1/3}$ is distance between centers of nearest atoms, k_p is packing index of nanocrystal structure. The function A_w arises due to taking into account the energy of „zero vibrations“ of atoms in the crystal:

$$A_w(k_n, R) = K_R\frac{5k_n ab(b+1)}{144(b-a)}R^{b+2},$$

$$K_R = \frac{\hbar^2}{k_B r_o^2 m}, \quad \xi = \frac{9}{k_n(\infty)}, \qquad (3)$$

where m is atom mass, $\hbar$ is Planck's constant, $k_n(\infty)$ is first coordination number in macrocrystal.

Let the considered nanocrystal is in vacuum and limited by Gibbs geometric surface. Also for atom interaction energy calculation we use the „only nearest neighbor interaction“approximation. Then the dependence of nanocrystal energy on size and shape will be determined by the dependence on size and shape of average (over the nanocrystal) value of first coordination number k_n. Under accepted assumptions, using for the oscillation spectrum of the nanocrystal the Einstein model, the specific (per atom) Helmholtz free energy of nanocrystal can be determined by the expression [11,13,14]:

$$f_H(k_n, R, T) = \left(\frac{k_n}{2}\right)D\cdot U(R) + 3k_B\Theta_E(k_n, R) \times\left\{\frac{1}{2} + \left(\frac{T}{\Theta_E(k_n, R)}\right)\ln\left[1 - \exp\left(-\frac{\Theta_E(k_n, R)}{T}\right)\right]\right\}. \qquad (4)$$

Here, Θ_E is Einstein temperature associated to Debye temperature by relationship [15]: $\Theta = (4/3)\Theta_E$, function of potential energy, as per (1), equal to:

$$U(R) = \frac{aR^b - bR^a}{b-a}.$$

Let's suppose the dependence of function k_n on size and shape of the nanocrystal with Gibbs surface does not depend on density and temperature, and is determined only by number of atoms in the nanocrystal, by parameter of its shape and constants $k_n(\infty)$ and k_p. Based on (4) for the equation of state and isothermal elastic modulus (B_T) one can obtain expressions [11,14]:

$$P = -\left(\frac{\partial f_H}{\partial v}\right)_T = \left[\frac{k_n}{6}D\cdot U'(R) + 3k_B\Theta_E\cdot\gamma\cdot E_w\left(\frac{\Theta_E}{T}\right)\right]\frac{1}{v}, \qquad (5)$$

$$B_T = -v\left(\frac{\partial P}{\partial v}\right)_T = P + \left[\frac{k_n}{18}D\cdot U''(R) + 3k_B\Theta_E \times\gamma(\gamma - q)\cdot E_w\left(\frac{\Theta_E}{T}\right) - 3k_B\cdot\gamma^2\cdot T\cdot F_E\left(\frac{\Theta_E}{T}\right)\right]\frac{1}{v}, \qquad (6)$$

The following functions are introduced here:

$$E_w(y) = 0.5 + \frac{1}{[\exp(y) - 1]},$$

$$F_E(y) = \frac{\partial E_w(y)}{\partial(1/y)} = \frac{y^2\exp(y)}{[\exp(y) - 1]^2},$$

$$U'(R) = R\left[\frac{\partial U(R)}{\partial R}\right] = \frac{ab(R^b - R^a)}{b-a},$$

$$U''(R) = R\left[\frac{\partial U'(R)}{\partial R}\right] = \frac{ab(bR^b - aR^a)}{b-a}. \qquad (7)$$

From Eq. (2) it is easy to find expressions for the first (γ) and second (q) Grüneisen parameters:

$$\gamma = -\left(\frac{\partial \ln\Theta}{\partial \ln v}\right)_T = \frac{b+2}{6(1+X_w)},$$

$$q = \left(\frac{\partial \ln\gamma}{\partial \ln v}\right)_T = \gamma\,\frac{X_w(1+2X_w)}{(1+X_w)}, \qquad (8)$$

where function is introduced: $X_w = A_w\xi/\Theta$, it determines the role of quantum effects in the crystal energy.

Since the function Θ in Eq. (2) does not depend on temperature during isochoric heating of the crystal, then isochoric and isobaric heat capacities can be determined in the form [15]:

$$C_v = 3N\cdot k_{\rm B}\cdot F_E\left(\Theta_{\rm E}/T\right),$$

$$C_p = C_v(1+\gamma\alpha_p T). \qquad (9)$$

The isobaric thermal volume-expansion coefficient can be calculated from the Grüneisen equation [15]:

$$\alpha_p = \frac{\gamma\cdot C_v}{V\cdot B_T} = \frac{\gamma\cdot C_v}{N\cdot B_T[\pi r_{\rm o}^3/(6k_p)]}\left(\frac{v_{\rm o}}{v}\right), \quad v_{\rm o} = \frac{\pi r_{\rm o}^3}{6k_p}. \qquad (10)$$

The obtained Eqs. (2)–(10) ensure calculation of the dependence of the both equation of state, and of the specified properties on the normalized volume: $v/v_{\rm o} = (c/r_{\rm o})^3 = R^{-3}$, temperature and $N-f$-arguments for single-component nanocrystal with specified structure (i.e. at given values $k_n(\infty)$ and k_p). At that it is necessary to know both parameters of interatomic potential (1), and $k_n(N, f)$ — functional dependence of the first coordination number on size and shape of the nanocrystal.

To determine the dependences of function k_n on size (i.e. number of atoms N) and shape of the nanocrystal we developed RP-model [13,14], its essence is as follows. Let us assume that nanocrystal with free Gibbs surface has the form of a rectangular parallelepiped with a square base, faceted by faces of the (100) type. The value $f = N_{ps}/N_{po}$ is a shape parameter, which is determined by the ratio of the number of atoms on the side edge N_{ps} to the number of atoms on the base edge N_{po}. For a rod-like shape $f > 1$, for a cube $f = 1$, for a plate-shaped nanocrystal $f < 1$. The number of atoms in nanocrystal is equal to: $N = fN_{po}^3/\alpha$, varies within: $2^3/\alpha \le N \le \infty$, where $\alpha = \pi/(6k_p)$ is structure parameter.

Note that shape of rectangular parallelepiped with square base is forced simplification. Actual nanocrystals have facet corresponding to their crystal structure and $P-T$-condition. But use of RP-model makes it possible the nanocrystal shape variation in isochoric-isomeric way. Just by this way the correct determination of both function $\sigma(T, v, N)$, and other properties of the nanocrystal was obtained in Refs. [10,11,13,14,16].

Within the framework of RP-model, the dependence of the normalized average (over the nanocrystal) value of the first coordination number on $N-f$-arguments has the form [13,14]:

$$k_n^* = \frac{k_n(N, f)}{k_n(\infty)} = 1 - Z_s(f)\left(\frac{\alpha^2}{N}\right)^{1/3}, \qquad (11)$$

where shape function is introduced:

$$Z_s(f) = \frac{1+2f}{3f^{2/3}}. \qquad (12)$$

The function (12) reaches a minimum equal to 1 at $f = 1$, i.e. for the cube shape. For plate ($f < 1$) or rod-like ($f > 1$) shapes, the $Z_s(f)$ value is greater than 1. Therefore, the function $k_n(f)^*$ from (11) at any N has a maximum at $f = 1$, i.e. for a cube, of the energy-optimal shape of rectangular parallelepiped. The volume and surface area for the RP-model are equal to [13,14]:

$$V = N_{po}^3 f c^3 = N\alpha c^3, \quad \Sigma = 6c^2\alpha_s(N\alpha)^{2/3}Z_s(f),$$

where α_s is coefficient considering density of atoms packing on the facet (i.e. in surface layer) of the nanocrystal: $\alpha_s \cong \alpha^{2/3}$. We can easily see that the volume of the nanocrystal V does not depend on the shape of the system, i.e. on the value f.

Within the RP-model, for the function $\sigma(N, f)$ — specific (per unit area) of free surface energy of the face (100) nanocrystal, isochoric and isobaric derivatives of function $\sigma(N, f)$ with respect to temperature and for surface pressure (P_{sf}) the following expressions [10,11,13,14,16] were obtained:

$$\sigma(N, f) = -\frac{k_n(\infty)DR^2}{12\alpha_s r_{\rm o}^2}\,L_E(N, f), \qquad (13)$$

$$\sigma'(T)_v = \left(\frac{\partial\sigma}{\partial T}\right)_{c,N,f} = -\frac{3k_{\rm B}R^2\gamma(N, f)}{2\alpha_s(b+2)r_{\rm o}^2k_n(N, f)^*}\,F_E\left(\frac{\Theta_{\rm E}}{T}\right), \qquad (14)$$

$$\sigma'(T)_P = \left(\frac{\partial\sigma}{\partial T}\right)_{P,N,f} = \sigma'(T)_v + v\cdot\alpha_p\left(\frac{\partial\sigma}{\partial v}\right)_{T,N,f}$$

$$= \sigma'(T)_v - \frac{2}{3}\,\sigma\cdot\alpha_p\cdot\Delta_p, \qquad (15)$$

$$P_{sf} = \left[\frac{\partial(\sigma\Sigma/N)}{\partial v}\right]_{T,N} = P_{\rm Ls}(1-\Delta_p). \qquad (16)$$

Here, the Laplace pressure ($P_{\rm Ls}$) and the functions introduced are written as:

$$P_{\rm Ls} = \frac{2\Sigma}{3V}\,\sigma = \frac{4\alpha_s Z_s(f)}{(\alpha N)^{1/3}c}\,\sigma = 4\alpha_s\frac{(1-k_n^*)}{\alpha c}\,\sigma, \qquad (17)$$

$$L_E(N, f) = U(R) + 3H_w(N, T), \qquad (18)$$

$$\Delta_p = -\frac{1}{2}\left[\frac{\partial\ln(\sigma)}{\partial\ln(c)}\right]_{T,N,k_p,f} = 1 + \frac{1}{2L_E(N, f)}$$

$$\times\left\{U'(R) - 9\left[q - \gamma\cdot t_y\left(\frac{\Theta_{\rm E}}{T}\right)\right]H_w(N, T)\right\}, \qquad (19)$$

$$H_w(N, T) = \frac{6\gamma(N, f)}{(b+2)}\left[\frac{k_B\Theta_E(N, f)}{Dk_n(N, f)}\right]E_w\left(\frac{\Theta_E}{T}\right),$$

$$t_y(y) = 1 - \frac{2y\exp(y)}{[\exp(2y)-1]}. \quad (20)$$

In „thermodynamic limit" (i.e. when $N \to \infty$ and $V \to \infty$ at $v = V/N = \text{const}$) from (11) we obtain $k_n^*(N \to \infty) \to 1$. Then functions P_{Ls} from (17) and P_{sf} from (16) disappear, and the Eqs. (13)–(15) transform into formulas for macrocrystal. At $T \to 0$ K functions from (14) and (15) aspire to zero at any values N or v, this is in agreement with third law of thermodynamics.

Note that surface pressure can be also determined using Eq. (5), as difference between pressures calculated for macro- and nanocrystal by formula:

$$P_{sf} = P(T, v, N = \infty) - P(T, v, N, f). \quad (21)$$

So, the obtained within the RP-model formulas from (1)–(20) ensure calculation of dependence of all lattice and surface properties on size and shape of the nanocrystal at any (corresponding to solid phase) P–T-conditions. Just by this method we studied changes of the both equation of state, and baric dependences of various properties during transition from macro- to nanocrystal with Gibbs free surface in Refs. [10,11,13,14,16]. In this review we present the results obtained for gold and compare them with modern state of calculations made by other authors.

3. Calculation results of gold nanocrystal properties

For calculations gold (Au, $m(\text{Au}) = 196.967$ a.m.u.) was selected as for the gold macrocrystal there are reliable experimental data used to test the calculation method. Gold is widely used in nanotechnologies and nanomedicine due to its low oxidability and well biocompatibility. Gold has a face-centered cubic (FCC) structure ($k_n(\infty) = 12$, $k_p = 0.7405$, $\alpha = \pi/(6k_p) = 0.70709$) and does not experience polymorphic phase transitions up to 220 GPa [17]. That is why the equation of state and baric dependences of the properties of FCC-Au macrocrystal are well studied and it is used as a pressure standard [18].

The parameters of pair interatomic potential (1) for FCC-Au were determined with the use of a self-consistency method in Ref. [16]. They have the following values:

$$r_o = 2.87 \cdot 10^{-10}\,\text{m},\ D/k_B = 7446.04\,\text{K},$$

$$b = 15.75, \quad a = 2.79. \quad (22)$$

The equation of state and properties of macrocrystal FCC-Au with parameters of interatomic potential (22) were calculated by us using the Eqs. (1)–(10) in Ref. [19]. As at $P = 0$ FCC-Au macrocrystal has a melting point equal to: $T_m(P = 0, N = \infty) = 1337$ K [20], so in Ref. [19] the baric and temperature dependences of various properties of FCC-Au were calculated in range of temperatures: $T = 10$–1337 K, and pressures: $P = 0$–110 GPa. The baric dependences obtained in [19] for FCC-Au macrocrystal showed good agreement with the experimental and theoretical results of other authors. Therefore, in this paper we used the potential parameters from (22).

We studied the change in baric dependences during the transition from macrocrystal to nanocrystal from $N = 306$ atoms. The $N = 306$ value was chosen for the following reasons. On the one hand, we wanted to illustrate most vividly the difference in the baric dependences for macro- and nano-size systems at various P–T-conditions. However, on the other hand, as it was shown experimentally in [21–24], and also by computer modeling in [25–27], and by the analytical method in [28–31], with the decrease in size of nanoparticle (nanocrystal or nanodroplet) with free surface, the parameters of the crystal–liquid phase transition (C–L PT) in it change. Moreover, at a certain number of atoms (N_0) the specific (per atom) latent heat of C–L PT disappears: $\Delta h(N_0) = 0$, and also jump in specific volume of C–L PT $\Delta v(N_0) = 0$. Thus, at $N \le N_0$ the phase difference disappears, and C–L PT is no longer possible here, since for such a cluster the thermodynamic concept of the solid or liquid phase is no longer applicable. At $P = 0$ the following estimates were theoretically obtained: for metals $N_0 = 300$ [25], 86 [26] and 50–300 [29]; for silicon: $N_0 = 23$–400 [30]. For FCC-argon by the analytical method using RP-model it was shown in Ref. [31] that S-loop of C–L PT on the isotherm of the equation of state disappears at the following cluster sizes:

$$N_0(T = 150\,\text{K}) = 485 \text{ (i.e. } N_{po} = 7)$$

$$N_0(T = 60\,\text{K}) = 38 \text{ (i.e. } N_{po} = 3).$$

Besides, we took the value $N = 306$ to study the influence of the nanocrystal shape on both the equation of state and the baric dependences of the lattice properties. The main calculations were made for nanocrystal of $N = fN_{po}^3/\alpha = 306$ atoms with the energy optimal shape of rectangular parallelepiped, i.e., with the shape of cube:

$$f = 1,\ N_{po} = 6, \quad k_n^* = 0.882152, \quad k_n = 10.5858.$$

However, some of the calculations were made for nanocrystal of same $N = fN_{po}^3/\alpha = 306$ atoms, but in the rod shape, i.e. at following values of parameters:

$$f = 8, \quad N_{po} = 3, \quad N_{ps} = N_{po}f = 24,$$

$$k_n^* = 0.833048, \quad k_n = 9.99658.$$

This allowed us to study the change in properties during an isothermal-isobaric change in the nanocrystal shape.

3.1. Equation of state

Modern literature presents many theoretical methods for size dependences calculation of various properties of nanocrystal at definite temperature. However, neither paper when studying the size dependence of properties did not

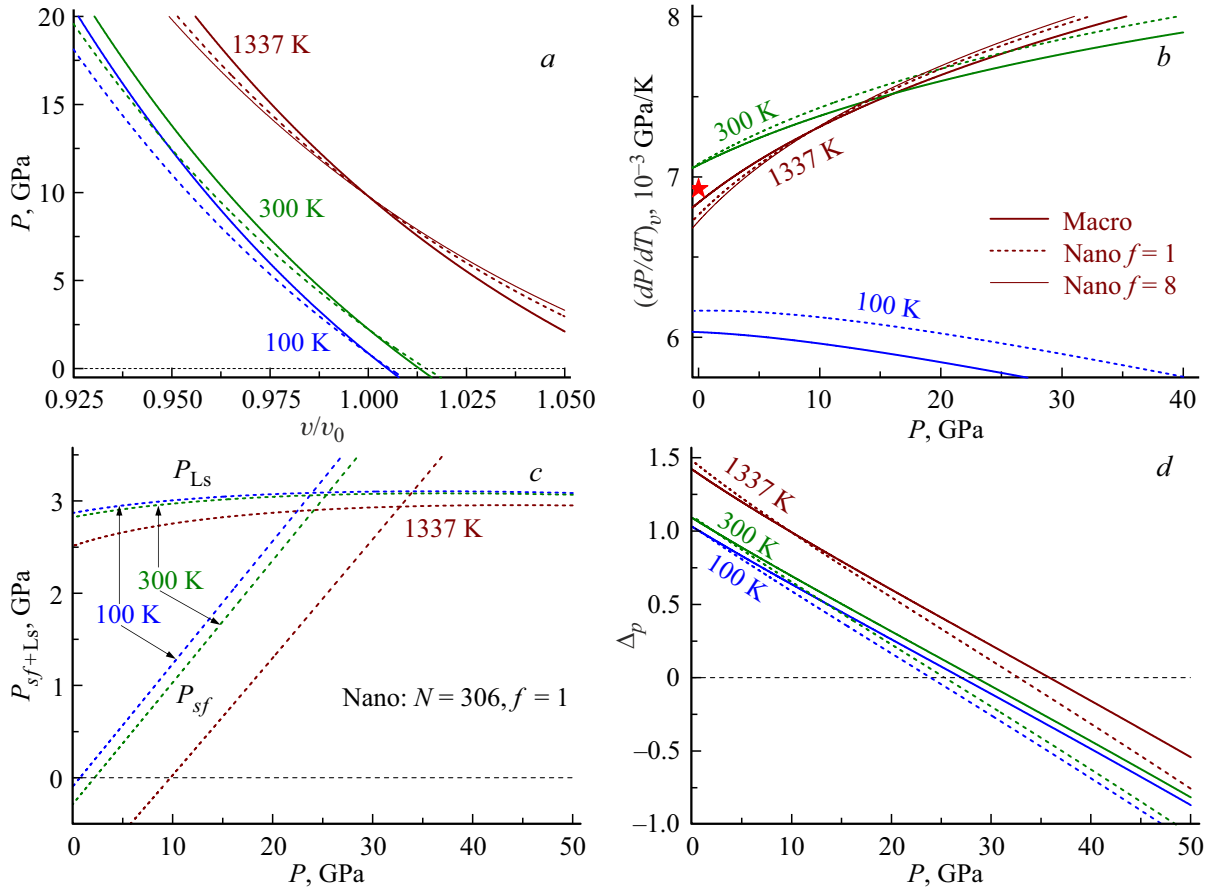

Figure 1. Isotherms of the equation of state (a) and isotherm baric dependences of following functions: b — for isochoric derivative $(\partial P/\partial T)_v$, c — for Laplace pressure and surface pressure, d — for function Δp from (19). Solid curves are calculations for macrocrystal, dashed lines are results for cubic nanocrystal. Thin solid line in Figures 1, a and b represents 1337 K isotherm for rod-like nanocrystal.

study the equation of state of nanocrystal, i. e. $P(v, T)$. At that in these papers (both with analytical and with computer calculations) by default it is assumed that with nanocrystal size decreasing in calculations $P = 0$ is fulfilled. However, they did not contain evidences of this equality. This resulted in wrong results, this was stated in by us in papers [10,32].

Figure 1, a shows the behavior of the thermal equation of state for FCC-Au, i. e. the isothermal dependences of the pressure (P, in GPa) on normalized volume ($v/v_o = (c/r_o)^3 = R^{-3}$) along three isotherms (bottom-up for a, b, d and top-down for c): 100, 300, 1337 K. Figure 1, b shows the baric dependence for the isochoric derivative $(\partial P/\partial T)_v$ (in 10^{-3} GPa/K), which was calculated by formula [15]: $(\partial P/\partial T)_v = \alpha_p \cdot B_T$. Solid thick curves show the results for macrocrystal, i. e. for $N = \infty$. The dashed lines show the results for cubic nanocrystal ($f = 1$) of 306 atoms. Thin solid line in Figures 1, a and b represents 1337 K isotherm for a rod-like ($f = 8$) nanocrystal of 306 atoms. The asterisk in Figure 1, b shows the result of calculating the $\alpha_p \cdot B_T$ value for FCC-Au macrocrystal at $P = 0$ and $T = 300$ K from Ref. [33]. Comparison of our calculated dependences $P(V)$ and $\alpha_p \cdot B_T(P, T)$ with experimental data for FCC-Au macrocrystal was provided in [19].

It is evident from Figure 1, a that isothermal dependences $P(v/v_o)$ for nano- and macrocrystals intersect at a certain value of relative volume $(v/v_o)_0$. So, in point: $(v/v_o)_0$, P_0, surface pressure becomes zero, i. e.: $P_{sf}(v/v_o)_0 = P(\text{Macro}) - P(\text{Nano}) = 0$. So, in this point, according to (19), the following is fulfilled: $\Delta_p(N, P_0) = 1$. This is shown in detail in Figure 1, c and d. At $P > P_0$ the surface pressure compresses the nanocrystal ($P_{sf} > 0$); and at $P < P_0$ the surface pressure stretches the nanocrystal: $P_{sf} < 0$. Calculations showed that P_0 decreases both at isomorphic-isomeric (f, N — const) increase in temperature, and at isomorphic-isothermal (f, T — const) decrease in N.

As can be seen from Figure 1, b at low temperatures $T < 100$ K the function $(\partial P/\partial T)_v$ increases both with isomorphic-isobaric decrease in the number of atoms N, and with isomeric-isobaric deviation of the nanocrystal shape from the energy optimal shape (for RP-model this is cube). However, at $T > 300$ K, the function $(\partial P/\partial T)_v$ depends weakly on the size and shape of the nanocrystal. In [19] it was shown that there is a certain temperature T_B, in the region of which the Birch approximation is satisfied, which assumes that at high temperatures the product $\alpha_p \cdot B_T$ does not depend on pressure. In this paper for FCC-Au macro-

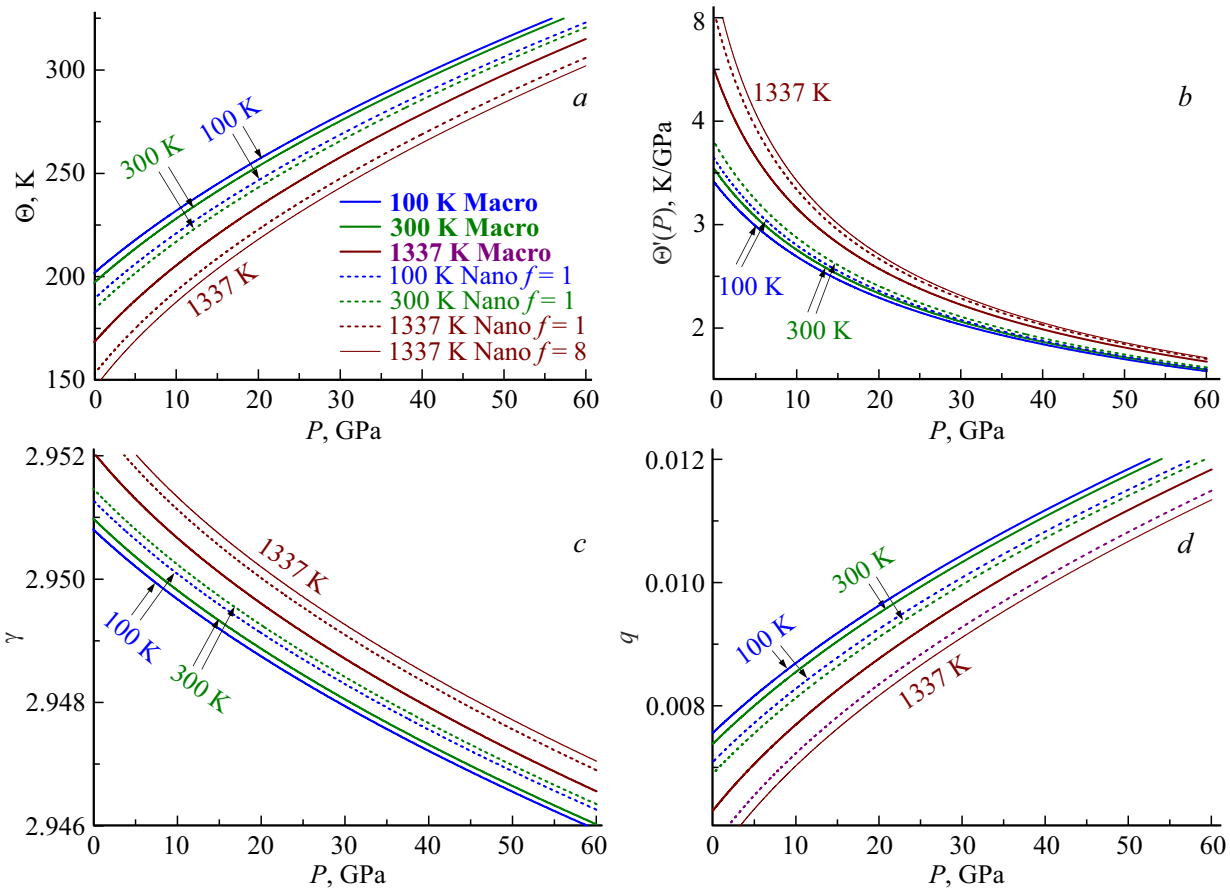

Figure 2. Isothermal baric dependences of functions: a — for Debye temperature Θ, b — for function $\Theta'(P)$ in K/GPa, c and d — for first γ and second q Grüneisen parameters. Solid curves are calculations for macrocrystal, dashed lines are results for cubic nanocrystal. The thin solid line represents the 1337 K isotherm for rod-like nanocrystal.

crystal we obtained: $T_B(N=\infty) = 137 \pm 15$ K. For cube nanocrystal FCC-Au of $N = 306$ atoms we obtained: $T_B(N = 306) = 131 \pm 15$ K. This indicates weak dependence of function $(\partial P/\partial T)_v = \alpha_p \cdot B_T$ on size and shape of nanocrystal at high temperatures.

Figure 1, c shows the isotherms of baric dependences of Laplace pressure from (17) (three top curves) and surface pressure from (16) (three bottom rising lines) for FCC-Au cube nanocrystal of $N = 306$ atoms. These functions were calculated along three isotherms (top-down): 100, 300, 1337 K. Figure 1, c and d shows that at pressure P_S the function $\Delta_p(N) = 1 - (P_{sf}/P_{\text{Ls}})$ from (19) changes sign. If at low pressures ($P < P_S$) the surface pressure is below the Laplace pressure: $P_{sf} < P_{\text{Ls}}$, i. e. $\Delta_p(N) > 0$, then at $P > P_S$ the surface pressure exceeds the Laplace pressure: $P_{sf} > P_{\text{Ls}}$, i. e. $\Delta_p(N) < 0$.

Figure 1, a and c show that at $P < P_0$ the surface pressure is negative: $P_{sf} < 0$, i. e. it stretches the nanocrystal. In addition to our papers [11,14], such behavior of surface pressure in nanocrystal was also obtained in the papers of other authors who used the analytical calculation method: for FCC-Au in [34], for BCC-Nb in [35], for BCC-W in [36], for BCC of substitutional alloy Mo –W in [37]. In Ref. [38] by means of molecular dynamics was studied the surface pressure for FCC-Ag nanocrystal of spherical shape. In [38] the transition of nanocrystal surface pressure to the negative region was also indicated. In the Ref. [39] it was shown that as the size of FCC-ruthenium (Ru) nanocrystal decreases at $P = 0$, the average interatomic distance in it increases. This also indicates that the nanocrystal is stretched by surface pressure.

3.2. Debye temperature and Grüneisen parameter

Size dependence of the Debye temperature was studied in many theoretical papers, but the baric dependence the $\Theta(N)$ function has not been studied due to the absence of the equation of state of the nanocrystal in these papers. So far, it has been possible to study the function $\Theta(N, f, P, T)$ only within the framework of RP-model.

Figure 2 shows isothermal baric dependences for functions: a — for Debye temperature Θ from (2), b — for derivative of function Θ with respect to pressure: $\Theta'(P) = (\partial\Theta/\partial P)_T$, in K/GPa, c and d — for the first γ and the second q Grüneisen parameters from (8). Calculations were performed along three isotherms (from top to bottom for a and d, from bottom to top for b and c): 100, 300, 1337 K. Solid curves correspond to the results of calculation

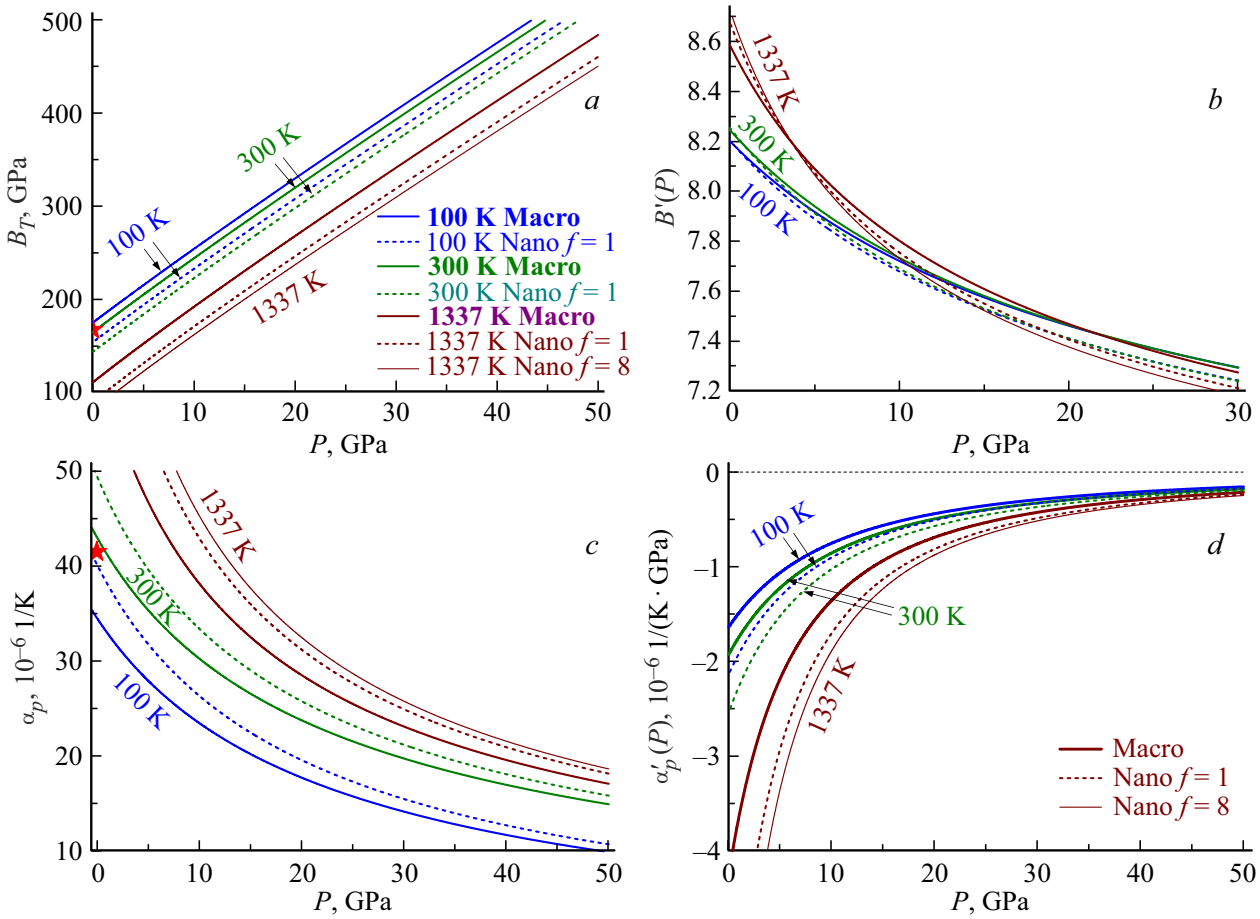

Figure 3. Isotherms of baric dependences of functions: *a* — for elastic modulus B_T in GPa, *b* — for function $B'(P)$, *c* — for thermal expansion coefficient α_p in 10^{-6} 1/K, *d* — for function $\alpha'_p(P)$ in 10^{-6} 1/(GPa K). Solid curves are the calculations for macrocrystal, and dashed are results for a cubic nanocrystal consisting of 306 atoms. The thin solid line represents the 1337 K isotherm for rod-like nanocrystal.

for macrocrystal, and dashed lines are results for cubic nanocrystal ($f = 1$) consisting of 306 atoms. Thin solid line represents 1337 K isotherm for rod-like ($f = 8$) nanocrystal of 306 atoms.

Figure 2 shows that during isomorphic-isothermal-isobaric decrease in nanocrystal size the values of Debye temperature Θ and second Grüneisen parameter q decrease, and values of $\Theta'(P)$ and first Grüneisen parameter γ increase at any pressure. The size dependence of these functions becomes more pronounced as the temperature rises and as the nanocrystal shape deviates further from the energy-optimal one (cubic for the RP model).

From Eqs. (2), (3) and (8) we can easily show that at limit compression, i. e. at $v/v_0 \to 0$, functions $\Theta(v)$ and $q(v)$ increase to maximum, and function $\gamma(v)$ decrease to zero [12]:

$$\lim_{v/v_0 \to 0} \Theta(v, N, f) = \Theta_{\max}(N, f) = \frac{4k_n(N, f)D}{9k_B},$$

$$\lim_{v/v_0 \to 0} \gamma = \gamma_{\min} = 0, \quad \lim_{v/v_0 \to 0} q = q_{\max} = \frac{b+2}{3}. \quad (23)$$

From (22) and (23) for macro- and nanocrystal FCC-Au we can obtain:

$$\Theta_{\max}(N = \infty) = 39712.2\,\text{K}, \quad q_{\max} = 5.917,$$

$$\Theta_{\max}(N = 306,\ f = 1) = 35034.1\,\text{K}.$$

Comparison of our calculated values Θ and γ for FCC-Au macrocrystal at $P = 0$ with experimental data was performed in Ref. [19]. At $P = 0$ the Θ decreasing for FCC-Au upon N decreasing was studied both theoretically in [40,41], and experimentally in [42]. However, the dependence of functions Θ and γ on size and shape of nanocrystal at various $P-T$-conditions was studied only by analytical method from (1)–(20) for FCC substitution alloy Au-Fe in [11], for Si in [14] and for BCC-Nb in [35]. Size changes for baric dependence of functions Θ, $\Theta'(P)$, γ and q for FCC-Au were studied by us for the first time.

3.3. Elastic modulus and thermal expansion coefficient

Figure 3 shows isotherms of baric dependence of the following functions: *a* — for isothermal elastic modulus:

$B_T = -v(\partial P/\partial v)_T$, in GPa, b — for baric derivative of elastic modulus: $B'(P) = (\partial B_T/\partial P)_T$, c — for thermal expansion coefficient: $\alpha_p = (\partial \ln v/\partial T)_P$, in 10^{-6} 1/K, d — for baric derivative of thermal expansion coefficient: $\alpha'_p(P) = (\partial \alpha_p/\partial P)_T$, in 10^{-6} 1/(GPa K). Calculations were performed in accordance with Eqs. (6) and (10) along three isotherms (from top to bottom, for a and d, from bottom to top for b and c): 100, 300, 1337 K. Solid curves are calculations for macrocrystal, dashed curves are results for cubic nanocrystal ($f = 1$) consisting of 306 atoms. Thin solid line represents 1337 K isotherm for rod-like ($f = 8$) nanocrystal of 306 atoms. Symbols in Figure 3, a and c show the calculation results for values of B_T and α_p for FCC-Au macrocrystal at $P = 0$ and $T = 300$ K from Ref. [33].

Figure 3, a, c and d shows that with isomorphic-isothermal-isobaric decrease in nanocrystal size the values B_T and $\alpha'_p(P)$ decrease, and value α_p increase at any pressure and temperature. The size variation of these functions becomes more pronounced as the temperature rises and as the nanocrystal shape deviates further from the energy-optimal one (cubic for the RP model). However, size dependence for the baric derivative $B'(P)$ is more complex. Figure 3, b shows that isothermal baric dependences of function $B'(P)$ for macro- and nanocrystal at a certain pressure (P_B) intersect, i. e. $B'(P_B)_\infty - B'(P_B)_N = 0$. At pressure P_B the size dependence of function $B'(P)$ changes its sign. At $P < P_B$ $B'(P)$ increases at isotherm-isobaric decrease in N, and at $P > P_B$ $B'(P)$ decreases.

Comparison of our calculated dependences $B_T(P, T)$, $B'(P)$ and $\alpha_p(P, T)$ with experimental data for FCC-Au macrocrystal was provided in [19]. Note that size change of functions B_T and α_p was studied in many papers (see, e. g., [11,38,41,43–48]). However, in these papers the dependence B_T and α_p on size of nanocrystal was studied either at $v = v_o$, or at $P = 0$. But $P = 0$ meeting upon decrease in nanocrystal size was not proved in these papers. As for size change of baric dependences B_T and α_p, and their baric derivatives $B'(P)$ and $\alpha'_p(P)$, the existing experimental or theoretical methods till now do not permit evaluation of these functions even at $P = 0$ and $T = 300$ K. However, the dependence of functions B_T, α_p, $B'(P)$ and $\alpha'_p(P)$ on the nanocrystal size at various $P-T$-conditions was studied by the analytical method from (1)–(20) for FCC substitution alloy in Au–Fe in [11], for Si in [14], for BCC-Nb in [35], for BCC-W in [36], for BCC of substitution alloy Mo–W in [37]. Size changes of baric dependence of functions B_T, α_p, $B'(P)$ and $\alpha'_p(P)$ for FCC-Au were studied by us for the first time. Under other methods (both analytical and computer simulation) this was not made yet.

3.4. Isochoric and isobaric thermal capacity

Figure 4 shows isotherms of baric dependence of following functions: a — normalized isochoric thermal capacity $C_v/(Nk_B)$, b — baric derivative of normalized isochoric thermal capacity: $C'_v(P)/(Nk_B) = (Nk_B)^{-1}(\partial C_v/\partial P)_T$, in 1/GPa, c — normalized isobaric thermal capacity $C_p/(Nk_B)$, d — baric derivative of normalized isobaric thermal capacity: $C'_p(P)/(Nk_B) = (Nk_B)^{-1}(\partial C_p/\partial P)_T$, in 1/GPa. Calculations were performed in accordance with formulas (9) along three isotherms (from bottom to top for a, b and c): 100, 300, 1337 K. Solid curves are calculations for macrocrystal, dashed curves are results for cubic nanocrystal ($f = 1$) consisting of 306 atoms. Thin solid line represents 1337 K isotherm for rod-like ($f = 8$) nanocrystal of 306 atoms. Symbols in Figure 4, a and c show the calculation results for values of $C_v/(Nk_B)$ and $C_p/(Nk_B)$ for FCC-Au macrocrystal at $P = 0$ and $P = 100$ GPa on isotherm $T = 300$ K from Ref. [33].

Comparison of our calculated dependences $C_v(P, T)$ and $C_p(P, T)$ with experimental data for FCC-Au macrocrystal was provided in [19]. In paper [45] we analytical showed that at $c = r_o$ the maximum of surface contribution into specific isochoric thermal capacity of the nanocrystal is reached at low temperature $T/\Theta = 0.2026$. With temperature rise the size change of isochoric thermal capacity disappears, this is the result of Dulong–Petit law: $C_v(T/\Theta \gg 1)/(Nk_B) = 3$. Figure 4 shows that effect of size on baric dependence of isobaric thermal capacity is maximum at high temperatures. But this size change decreases with pressure rise.

The Refs. [40,43,46–49] evaluated the size change of thermal capacity at $c = r_o$. However, in these papers the equation of state of nanocrystal was not studied. So, evaluations of size contribution into the isobaric thermal capacity are approximate in these papers. Due to same reason in publications there are no data in size change of baric derivatives of isochoric and isobaric thermal capacities of nanocrystals. The dependence of function C_p on nanocrystal size at various $P-T$-conditions was studied only by analytical method from (1)–(20) for FCC substitution alloy in Au–Fe in [11], for Si in [14], for BCC-W in [36] and for BCC of substitution alloy Mo–W in [37]. Size changes of baric dependence of functions C_v, C_p, $C'_v(P)$ and $C'_p(P)$ for FCC-Au were studied by us for the first time.

3.5. Specific free surface energy

Review of modern calculation methods for specific free surface energy (hereinafter referred to as specific surface energy) for both macro-, and nanocrystals was made by us in Refs. [10,16,32]. However, as these papers do not contain the equation of state, it is unclear — whether the values of $\sigma(T)$ obtained in these papers correspond to the isobar $P = 0$?

Figure 5 shows isotherms of baric dependence (a and c) and isobars of temperature dependence (b and d) for specific surface energy σ of facet (100) in 10^{-3} J/m^2 (a and b), and derivative of function $\sigma(100)$ with respect to pressure $\sigma(P)$ in 10^{-3} J/(m^2 GPa) (c and d). Calculations were performed in accordance with Eq. (13) along three isotherms (from top to bottom, for a, from bottom to top for c): 100, 300, 1337 K, and along three isobars (from bottom to top for b, from top to bottom for d): 0, 24,

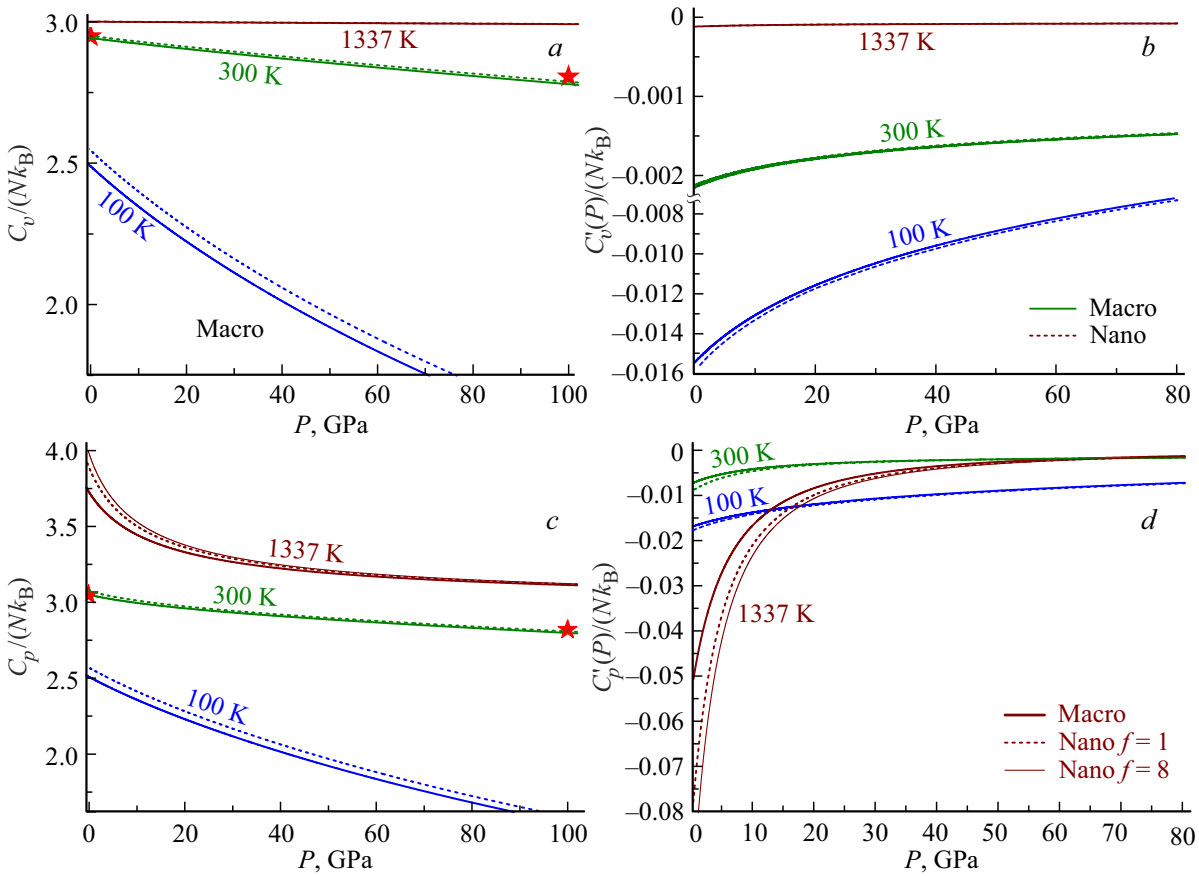

Figure 4. Isotherms of baric dependence of functions: a — for normalized isochoric thermal capacity $C_v/(Nk_B)$, b — for function $C'_v(P)/(Nk_B)$ in 1/GPa, c — for normalized isobaric thermal capacity $C_p/(Nk_B)$, d — for function $C'_p(P)/(Nk_B)$ in 1/GPa. Solid curves are calculations for macrocrystal, dashed lines are results for cubic nanocrystal. The thin solid line represents the 1337 K isotherm for rod-like nanocrystal. Symbols in Figure 4, a and c show the calculation results for FCC-Au macrocrystal from [33].

60 GPa. Solid curves are calculations for macrocrystal, dashed curves are results for cubic nanocrystal ($f = 1$) consisting of 306 atoms. Thin solid curves in Figure 5, a and c represent the 1337 K isotherm for rod-like nanocrystal ($f = 8$) of 306 atoms. Comparison of our calculated values $\sigma(100)$ for FCC-Au macrocrystal at $P = 0$ with evaluations made by other authors was performed in Refs. [16,19].

From Figure 5, a and b we see that at $P = 0$, the σ value decreases with decreasing N, the more noticeably the higher the temperature. However, at low temperatures and high pressures on isotherm there are two P-points, where the specific surface energy does not depend on the nanocrystal size: $\sigma(N) = \sigma(\infty)$. With temperature rise these P-points approach each other, and at high temperatures such P-points are not observed on the isotherm. In region, enclosed by P-points value σ increases with isothermal-isobaric decrease in nanocrystal size. Such function $\sigma(P, N)$ behaviour is due that at low temperatures, with increasing pressure, the surface pressure compresses the nanocrystal (see Figure 1, c). This results in more noticeable rise of function $\sigma(N)$ with pressure as compared to rise of function $\sigma(\infty)$. So, the first P-point appears, as well as region, where the following is met: $\sigma(N) > \sigma(\infty)$. With pressure rise the function $\sigma(N)$ reaches maximum at lower pressure than function $\sigma(\infty)$. This results in second P-point formation on the isotherm. During isobaric rise of temperature the function $\sigma(N)$ decreases more than function $\sigma(\infty)$. As result the region with P-points disappears at high temperatures.

It can be seen from Figure 5, b and c that $\sigma'(P)_T$ increases with isomorphic-isomeric-isobaric temperature rise. At that on isotherm at definite pressure (P_σ) there is a point, where the baric dependences $\sigma'(P)_T$ for macro- and nanocrystal intersect, i. e. $\sigma'(P_\sigma)_{T,\infty} - \sigma'(P_\sigma)_{T,N} = 0$. In these crossing points the size dependence of function $\sigma'(P)_T$ changes. At $P < P_\sigma$ the function $\sigma'(P)_T$ rises upon isothermal-isobaric decrease of N, and at $P > P_\sigma$ the function $\sigma'(P)_T$ decreases. Here we see the analogy between baric dependences of function $\sigma'(P)_T$ from Figure 5, b and function $B'(P)$ from Figure 3, b.

We see from Eq. (13) that at strong isothermal compressions or stretchings, or at large isobaric heating of the crystal the function $\sigma(P)$ transits in negative region. It is easy to understand that at $\sigma < 0$ fragmentation shall start, i. e. the crystal will aspire to increase in any way its specific (per atom) surface: either free (under stretching), or intercrystalline (under compression). The conditions of baric and temperature fragmentation of the crystal were considered by us in detail in Ref. [14].

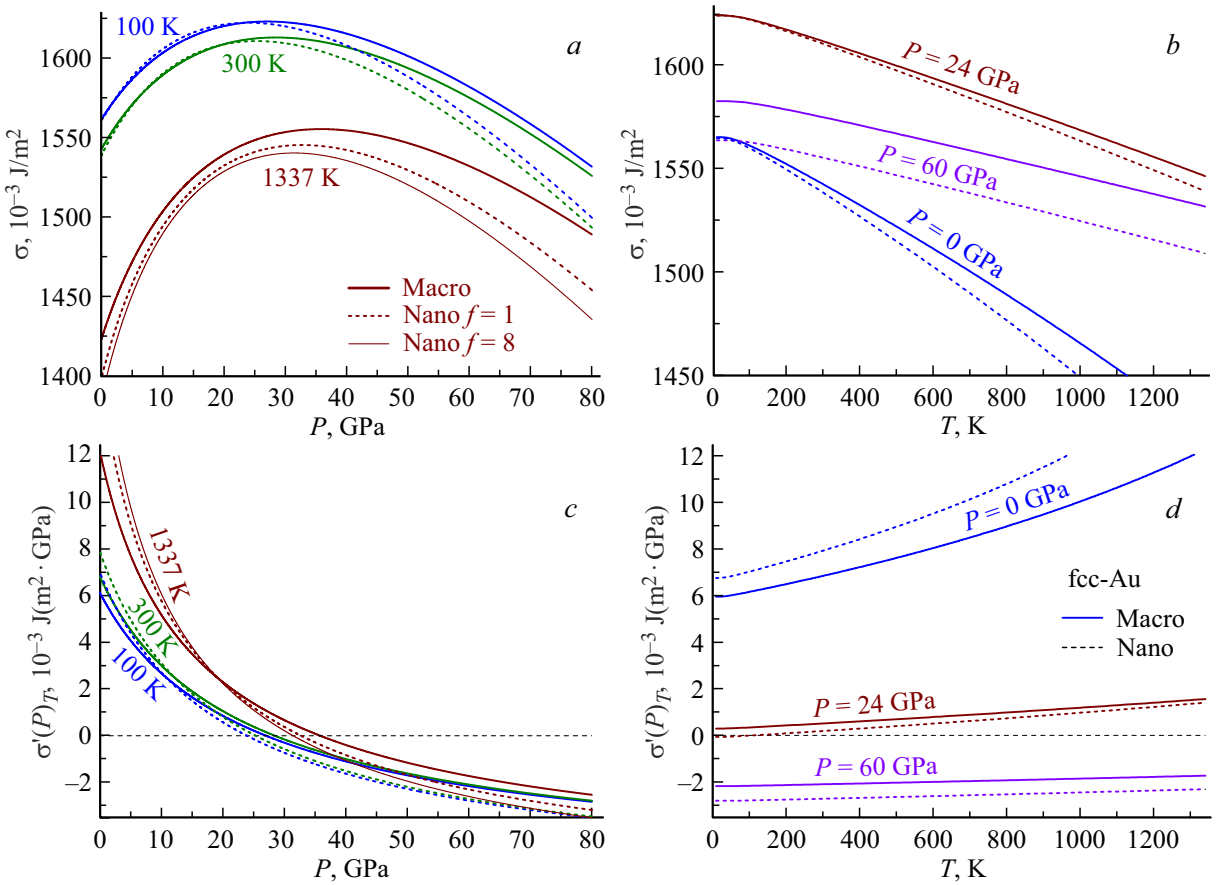

Figure 5. Isotherms of baric dependence (a and c) and isobars of temperature dependence (b and d) for specific surface energy σ in 10^{-3} J/m^2 (a and b), and derivative of function σ with respect to pressure $\sigma'(P)$ in 10^{-3} J/(m^2 GPa) (c and d). Solid curves are calculations for macrocrystal, dashed lines are results for cubic nanocrystal. Thin solid line in Figure 5, a and c represent the 1337 K isotherm for rod-like nanocrystal.

3.6. Derivatives of specific surface energy with respect to temperature

Figure 6 shows isotherms of baric dependence (a and c) and isobars of temperature dependence (b and d) for isochoric derivatives of specific surface energy with respect to temperature, i. e. for function $\sigma'(T)_v$ (a and b), and function $\sigma'(T)_P$ (c and d). Both functions are in 10^{-6} J/(m^2 K). Calculations were performed in accordance with Eqs. (14) and (15) along three isotherms (from top to bottom, for a and c): 100, 300, and 1337 K, and along three isobars (from bottom to top, for d): 0, 24, 60 GPa. Solid curves correspond to the results of calculation for macrocrystal, and dashed lines are results for cubic nanocrystal ($f = 1$) consisting of 306 atoms. Thin solid line in Figure 6, a and c represents 1337 K isotherm for rod-like ($f = 8$) nanocrystal of 306 atoms. Comparison of our calculated values $\sigma'(T)_P$ for FCC-Au macrocrystal at $P = 0$ with evaluations made by other authors was performed in Refs. [16,19].

Figure 6 shows that during isomorphic-isothermal-isobaric decrease in nanocrystal size $|\sigma'(T)_v|$ and $|\sigma'(T)_P|$ increase at any $P-T$-conditions. The size changes of these functions becomes more noticeable as the temperature rises and at the nanocrystal shape deviates from the energy-optimal one (cubic for the RP model). At low pressures $|\sigma'(T)_v| < |\sigma'(T)_P|$ is fulfilled. However, at high pressures this inequality changes to opposite. Therefore, one should not equate functions $\sigma'(T)_v$ and $\sigma'(T)_P$, as it is done in certain studies. At $T \gg \Theta$ and low pressures the function $\sigma'(T)_v$ is almost independent of temperature, and $|\sigma'(T)_P|$ is greater the higher the temperature is.

As it was noted in Ref. [45], function σ at $T = 0$ K shall satisfy the following conditions ($i = v$ or P) to adhere to the third law of thermodynamics:

$$\lim_{T\to 0K}\left(\frac{\partial\sigma}{\partial T}\right)_{i,N} = -0,$$

$$\lim_{T\to 0K}\left[\frac{\partial(\partial\sigma/\partial T)_{v,N}}{\partial v}\right]_{T,N} = -0,$$

$$\lim_{T\to 0K} T\left[\frac{\partial}{\partial T}\left(\frac{\partial\sigma}{\partial T}\right)_{v,N}\right]_{i,N} = -0. \qquad (24)$$

Conditions (24) are valid for any crystal structure, at any specific volume and pressure, and for any size and shape of the nanocrystal. At the same time, in some papers for the

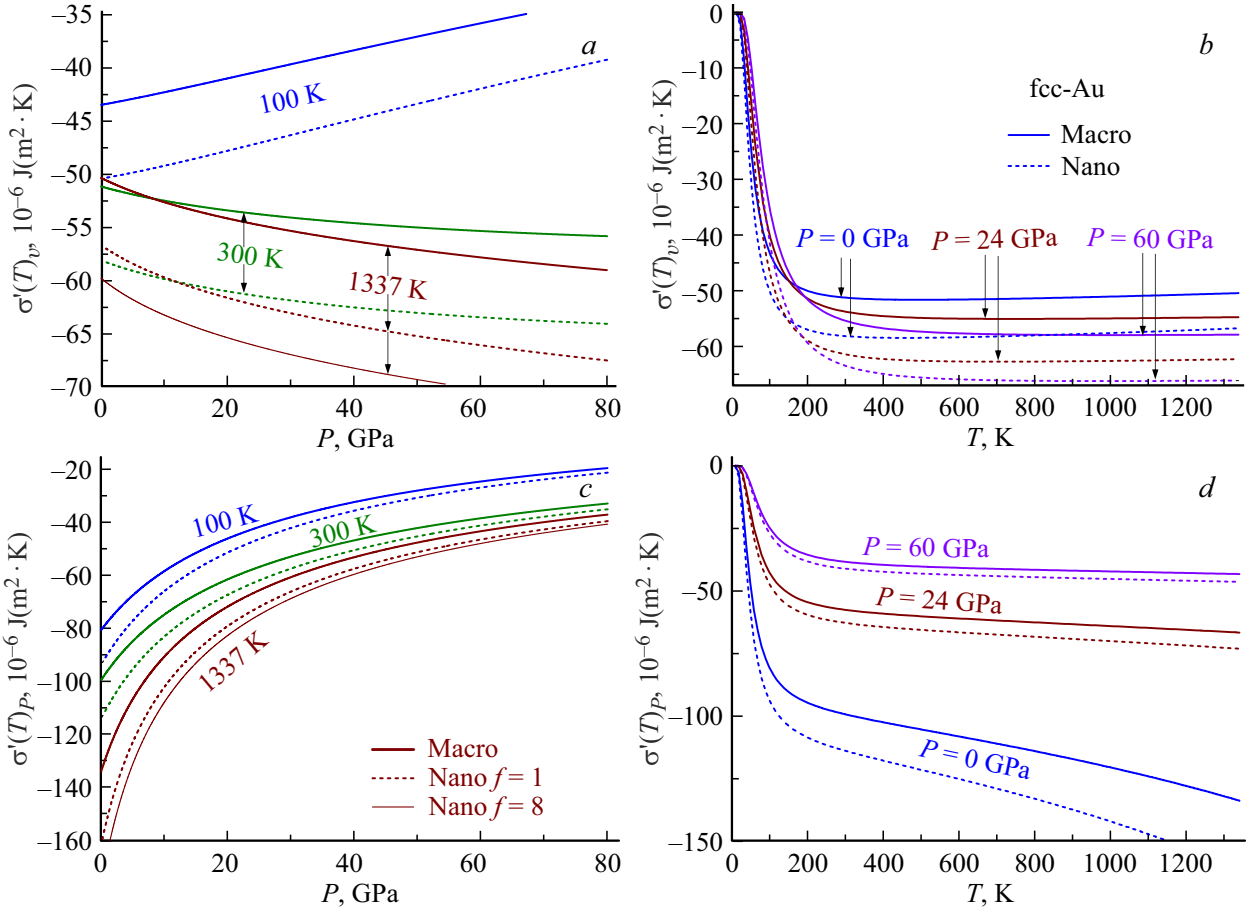

Figure 6. Isotherms of baric dependence (a and c) and isobars of temperature dependence (b and d) for function $\sigma'(T)_v$ (a and b), and function $\sigma'(T)_P$ (c and d), both functions in 10^{-6} J/(m^2 K). Solid curves are calculations for macrocrystal, dashed lines are results for cubic nanocrystal. Thin solid line in Figure 6, a and c represent the 1337 K isotherm for rod-like nanocrystal.

temperature dependence $\sigma(T)$ the linear approximation of the following form was used [4,6]:

$$\sigma(T) = \sigma(T = 0\,\mathrm{K}) - \mathrm{const} \cdot T. \qquad (25)$$

However, it follows from Figure 6 the approximation (25) is valid at high temperatures only: $T \gg \Theta$ (for $i = v$) or at high pressures (for $i = v$ or $i = P$). The use of approximation (25) at low temperatures can lead both to numerical errors and to violation of the third law of thermodynamics (24).

Different methods for calculation of the derivative of function σ with respect to temperature for macrocrystal at $P = 0$ were suggested (see, for example, Ref. [4–6,50–55]). However, since the equation of state considering the surface was not given in these studies, it remains unclear whether the obtained in these papers value $\sigma'(T)$ is an isochoric derivative or isobaric one. At the same time, it can be seen from Figure 6 that the difference between functions $\sigma'(T)_v$ and $\sigma'(T)_P$ is significant, especially at $P = 0$.

The specific surface energy decreasing with the nanocrystal size decreasing at $P = 0$ was obtained also in theoretical papers of other authors [7,8,40,49,56] (although the equality $P = 0$ was not proved in these papers). However, size dependence of functions $\sigma(P)$ and $\sigma'(P)$ was studied by analytical method from (1)–(20) only for FCC substitution alloy in Au–Fe [11], for Si in [14], for FCC-Rh in [16], for BCC-Nb in [35], for BCC-W in [36], and for BCC substitution alloy Mo–W in [37]. These data are not yet obtained by other methods (both analytical and computer). The problem here is related to the fact that in the theoretical models within which the function σ was calculated, the equation of state of the crystal taking into account the surface was not obtained. Meanwhile, the dependence $\sigma(P)$ is necessary for studying both the crack initiation under baric action on the macrocrystal, and for obtaining the equation of state for the nanocrystal. The size changes of baric dependence of functions σ, $\sigma'(P)$, $\sigma'(T)_v$ and $\sigma'(T)_P$ for FCC-Au were studied by us for the first time.

3.7. Baric dependence of melting point

The melt point is single parameter, which the size dependence can be experimentally measured [57,58]. That's why various calculation methods for nanocrystal properties were

checked exactly during calculation of the size dependence of melt point. However, it was not possible to prove that the dependence $T_m(N)$ obtained in these papers is an isobaric size dependence in these papers.

There is no melting theory [59], so to study the size dependence of the melt point various empiric criteria are used. In the Ref. [60], based on the method from Ref. [19] and the delocalization criterion for the phase transition crystal-liquid from Refs. [59,61], the expression was obtained to calculate the baric dependence of the melting point (T_m) for single-component macrocrystal, which has the form:

$$T_m(P) = T_m(P, T_m(0)) \times \exp\Big[-\frac{b}{3}\alpha_p(P, T_m(0))[T_m(P, T_m(0)) - T_m(0)]\Big], \quad (26)$$

where $T_m(0)$ — melting point of macrocrystal at $P = 0$, $\alpha_p(P, T_m(0))$ — thermal volumetric expansion coefficient at pressure P, calculated along the isotherm $T_m(0)$ [19,60],

$$T_m(P, T_m(0)) = T_m(0) \cdot \left[\frac{c_o(P, T_m(0)) \cdot \Theta_o(P, T_m(0))}{c_o(0, T_m(0)) \cdot \Theta_o(0, T_m(0))}\right]^2 \times \frac{f_y(y_w(P, T_m(0)))}{f_y(y_w(0, T_m(0)))}. \quad (27)$$

Function $f_y(y_w)$ appears in (27) in order to consider quantum effects and is written as [60]:

$$f_y(y_w) = \frac{2}{y_w}\frac{[1 - \exp(-y_w)]}{[1 + \exp(-y_w)]}, \quad y_w = \frac{\Theta_E}{T} = \frac{3\Theta}{4T}. \quad (28)$$

Within RP-model the baric dependence of the melting point from (26) can be summarized for the case of nanocrystal of N atoms in the form [62]:

$$T_m(P, N) = T_m(P, T_m(0), N) \exp\Big[-\frac{b}{3}\alpha_p(P, T_m(0), N) \times [T_m(P, T_m(0), N) - T_m(0, T_m(0), N)]\Big], \quad (29)$$

Here, we introduce functions that are summarized (27) for the case of nanocrystal:

$$T_m(P, T_m(0), N) = T_m(0, T_m(0), N) \times \left[\frac{c_o(P, T_m(0), N) \cdot \Theta_o(P, T_m(0), N)}{c_o(0, T_m(0), N) \cdot \Theta_o(0, T_m(0), N)}\right]^2 \times \frac{f_y(y_w(P, T_m(0), N))}{f_y(y_w(0, T_m(0), N))}. \quad (30)$$

$$T_m(0, T_m(0), N) = T_m(0) \times \left[\frac{c_o(0, T_m(0), N) \cdot \Theta_o(0, T_m(0), N)}{c_o(0, T_m(0), \infty) \cdot \Theta_o(0, T_m(0), \infty)}\right]^2 \times \frac{f_y(y_w(0, T_m(0), N))}{f_y(y_w(0, T_m(0), \infty))}. \quad (31)$$

In „thermodynamic limit“ (i. e. when $N \to \infty$ and $V \to \infty$ at $v = V/N = \text{const}$) from (12) we obtain $k_n^*(N \to \infty) = 1$. Then from (31) we obtain $T_m(0, T_m(0), N \to \infty) = T_m(0)$, and Eq. (30) transits into function (27).

When using potential parameters (22), by Eqs. (3)–(20) for parameters included in formulas (30) and (31) along isotherm $T_m(0) = 1337\,\text{K}$ at $P = 0$ we obtained:

for macrocrystal:

$$c_o(0, T_m(0), \infty) = 2.93432 \cdot 10^{-10}\,\text{m},$$

$$\Theta_o(0, T_m(0), \infty) = 168.280\,\text{K},$$

for nano-cube:

$$c_o(0, T_m(0), 306, 1) = 2.94560 \cdot 10^{-10}\,\text{m},$$

$$\Theta_o(0, T_m(0), 306, 1) = 152.793\,\text{K},$$

for nano-rod:

$$c_o(0, T_m(0), 306, 8) = 2.95162 \cdot 10^{-10}\,\text{m},$$

$$\Theta_o(0, T_m(0), 306, 8) = 145.823\,\text{K}.$$

Using these values and Eqs. (3)–(20), in Ref. [62] the baric dependences of the melting point were calculated for both macro- and nanocrystals of 306 atoms with cube and rod-like surfaces.

Figure 7 shows baric dependences both for the melting temperature $T_m(P)$ (a and c), and for the melting temperature derivative with respect to pressure: $T'_m(P) = dT_m/dP$ (b and d) in K/GPa. Function $T'_m(P)$ was calculated by means of numerical differentiation of isothermal dependence from (29) with respect to pressure. In Figure 7 the solid and dashed lines show the experimental dependences for the FCC-Au macrocrystal from Refs. [63] and [20], respectively. These experimental data were approximated by the Simon–Glatzel equation – of the following form:

$$T_m(P) = T_{m0}\left[1 + \frac{P}{P_0}\right]^{c_s}, \quad (32)$$

$$T'_m(P) = \frac{dT_m(P)}{dP} = T_{m0}\frac{c_s}{P_0}\left[1 + \frac{P}{P_0}\right]^{c_s - 1}. \quad (33)$$

In Ref. [63] for FCC-Au for the pressure region up to 6 GPa we obtained:

$$T_{m0} = 1339\,\text{K},\ P_0 = 16.1\,\text{GPa},\ c_s = 0.57$$

— solid line in Figure 7.

In Ref. [20] for FCC-Au for the pressure region up to 106 GPa were obtained:

$$T_{m0} = 1337\,\text{K},\ P_0 = 22.265 \pm 1.83\,\text{GPa},\ c_s = 0.662 \pm 0.03$$

— dashed line in Figure 7.

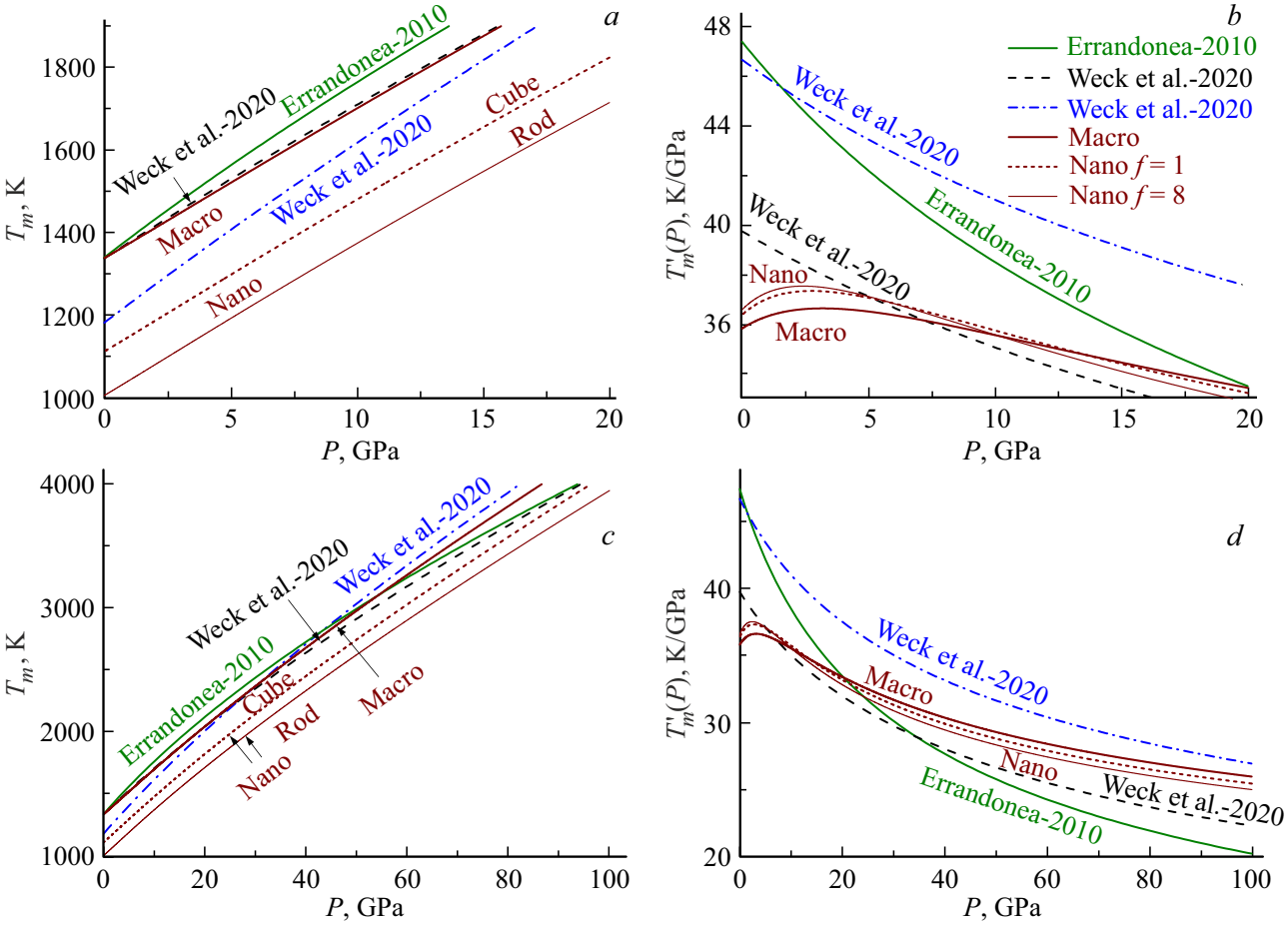

Figure 7. Baric dependence of the melting point $T_m(P)$ (a and c), and its derivative with respect to pressure $T'_m(P)$ (b and d) for FCC-Au. The upper graphs show the low pressure region: $P = 0-20$ GPa, and in bottom graphs the range $P = 0-100$ GPa is shown.

Also in the Ref. [20] the dependence $T_m(P, \infty)$ for FCC-Au was calculated using the molecular dynamics simulations. For the pressure range up to 107 GPa were obtained:

$$T_{m0} = 1181\,\text{K},\ P_0 = 17.94\,\text{GPa},\ c_s = 0.709.$$

This calculated dependence is shown in Figure 7 by dash-dotted line.

Our calculation for macrocrystal is shown by solid thick line, which practically merges with the experimental dependence $T_m(P)$ from Ref. [20]. The dotted line shows our calculations for cube nanocrystal of 306 atoms. The thin solid line shows our calculations for rod-like nanocrystal of 306 atoms.

From Figure 7, a and c we see that our dependence $T_m(P)$ for the macrocrystal is in better agreement with the experimental dependences from Refs. [20,63], than dependence obtained in Ref. [20] by molecular dynamics simulations up to 100 GPa. As can be seen from Figure 7, a and c the dependence $T_m(P)$ for the nanocrystal lays below the dependence for macrocrystal. Moreover, the difference $T_m(P, \infty) - T_m(P, N)$ is greater, the greater the nanocrystal shape deviates from the energy optimal shape (for RP-model this is cube). This is in agreement with experimental and theoretical results obtained in Refs. [26,29,34,40,43,46,49,64–69] for FCC metals at $P = 0$ (although the equality $P = 0$ was not proved in these papers). From Figure 7, a it also follows that during isobaric heating of an array of isomeric (i. e. with the same number of atoms N) nanocrystals the nanocrystals, whose shape deviates most from the energy optimal shape, will melt first. Nanocrystals with energy optimal shape have maximum melting point for a given number of atoms. This was first stated in the Ref. [13]. In this case, the shape relaxation can occur, i. e., nanocrystal with „non-optimal“ shape, having melted, can immediately crystallize into a more „refractory“ energy optimal shape.

As can be seen from Figure 7, b the baric dependences of the functions $T'_m(P)$ for cube macro- and nanocrystal intersect at the point: $P_x = 13.63$ GPa, $T'_m(P)_x = 34.75$ K/GPa. This means that at low pressures $T'_m(P)$ increases, and at $P > P_x$ $T'_m(P)$ decreases upon isomorphic-isobaric decrease in the nanocrystal size. However, as can be seen from Figure 7, the dependence of the function $T'_m(P)$ on size and shape is insignificant. This indicates that, with

constant $N-f$-arguments the baric dependences $T_m(P, \infty)$ and $T_m(P, N, f)$ are practically parallel.

Note that the dependences of the melting point on size and shape at various pressures were also studied by the analytical method from (1)–(20) for Si in [14,30], for FCC-Au in [34], for BCC-Nb in [35], and for BCC-Mo in [70]. However, in these papers a simplified formula was used to calculate the dependence $T_m(P, N)$, which we described in detail in Ref. [56]. Therefore, the agreement with the experimental data for macrocrystal in these papers was worse than that shown in Figure 7.

The experimental and theoretical determination of the dependence $T_m(N)$ even at $P = 0$ is a very difficult task [64–69]. Therefore, in the literature there are many different dependencies $T_m(P = 0, N)$, which lie in a wide range of values [34,64–69]. For example, according to estimates from [64] (Figure 2), for a spherical Au nanoparticle with a radius of 1.1 nm (i.e. of $N = 309$ atoms) „surface melting temperature" lies in the range: $T_m(P = 0, N = 309)_{\text{surf}} = 473-873$ K, and „core melting temperature" of nanoparticles is by 200–250 K higher. Thus, the entire Au nanocrystal of 309 atoms will melt after 1073–1123 K. In our calculations for homogeneous nanocrystal with geometric Gibbs surface, we obtained (Figure 7, *a*):

for cube shape:

$$T_m(P = 0, N = 306, f = 1) = 1111.34\,\text{K},$$

for rod-like shape:

$$T_m(P = 0, N = 306, f = 8) = 1004.58\,\text{K}.$$

So, the obtained value of $T_m(P = 0, N = 306, f = 1)$ is in good agreement with the melting point of the entire nanocrystal of 309 atoms, obtained in Ref. [64]. This confirms not only the calculation method for size dependence of the melting point, but also the used here method of dependence calculation of all lattice properties of the nanocrystal both on its size, and shape of its surface.

4. Discussion of results

For almost all metals the energy of a pair interatomic bond is much greater than the energy of „zero" vibrations of atoms, i.e., the condition is satisfied:

$$\frac{8D}{k_{\text{B}}A_w(k_n, c)\xi^2} \gg 1.$$

Then formula (4) can be simplified to form:

$$\Theta(k_n, c) \cong \left[\frac{8DA_w(k_n, c)}{k_{\text{B}}}\right]^{1/2} = \left[\frac{5\hbar^2 D k_n a b(b+1)}{18k_{\text{B}}^2 m r_{\text{o}}^2 (b-a)}\left(\frac{r_{\text{o}}}{c}\right)^{b+2}\right]^{1/2},$$

$$\Theta^* = \frac{\Theta(N, R)}{\Theta(\infty, 1)} \cong (k_n^*)^{1/2} R^{(b+2)/2}. \qquad (34)$$

For the function: $X_w = A_w\xi/\Theta$, which is included in (8), we can easily obtain:

$$X_w(N, R) = \frac{A_w(N, R)\xi}{\Theta(N, R)} \cong X_w(\infty, 1) \cdot (k_n^*)^{1/2} R^{(b+2)/2},$$

where designation are introduced:

$$X_w(\infty, 1) = \frac{A_w(\infty, 1)\xi}{\Theta(\infty, 1)} \cong \left[\frac{\xi^2 k_B A_w(\infty, 1)}{8D}\right]^{1/2} \ll 1.$$

Then for the first, second and third Grüneisen parameters we can obtain:

$$\gamma(N, R) \cong \frac{b+2}{6}\left[1 + X_w(\infty, 1) \cdot (k_n^*)^{1/2} R^{(b+2)/2}\right]^{-1},$$

$$q(N, R) \cong \gamma X_w(N, R) \cong q(\infty, 1) \cdot (k_n^*)^{1/2} R^{(b+2)/2},$$

$$z(N, R) = -\left(\frac{\partial \ln q}{\partial \ln v}\right)_T = \frac{(b+2)}{6}\frac{(1+3X_w)}{(1+X_w)^2} \cong \frac{(b+2)}{6}\left[1 + X_w(\infty, 1) \cdot (k_n^*)^{1/2} R^{(b+2)/2}\right], \qquad (35)$$

where: $q(\infty, 1) \cong \gamma(\infty, 1) X_w(\infty, 1)$.

Figure 8 shows the isochoric (at $R = 1$) dependences of normalized (to values for macrocrystal) functions: k_n^* from (11), A_w^* from (3), Θ^* from (2), γ^*, q^* from (8) and z^* from (35) of argument $1/N^{1/3}$. Solid symbols connected by solid lines are obtained for cube shape, i.e. at $f = 1$. Open symbols connected by dashed lines were obtained for rod-like shape at $f = 8$. Here, $F^* = F(N, R)/F(N = \infty, R = 1)$. Symbols on isomorphs indicate position of permitted (at given f) number of atoms in nanocrystal: $N = fN_{po}^3/\alpha$, where $N_{po} = 2, 3, 4, \ldots$ — number of atoms on edge of square base of parallelepiped. Calculations are made for FCC-Au nanocrystal with potential parameters from (22). From Figure 8 we see that if crystal shape deviates from energy optimal shape (for RP-model this is cube) the size dependences amplify. At that, for the first and third Grüneisen parameters the size dependences are insignificant as compared to other functions.

Function k_n^* from (11) decreasing results in inclination decreasing of function $P(v/v_{\text{o}})$ from (5), and function Θ^* from (2) decreasing results in $v(P = 0)/v_{\text{o}}$ increasing, see Figure 1. That's why for nanocrystal value of $P = 0$ is reached at higher specific volume, i.e. relationship is satisfied:

$$\left(\frac{v(P=0)}{v_{\text{o}}}\right)_{\text{Nano}} > \left(\frac{v(P=0)}{v_{\text{o}}}\right)_{\text{Macro}}.$$

This inequality agrees with the results of experimental and theoretical papers [39,71–75].

Such change of function $P(v/v_{\text{o}})$ results in decrease in isothermal elastic modulus B_T from (6), see Figure 2. Decrease in elastic modulus during isothermal decrease in nanocrystal size was also obtained in theoretical

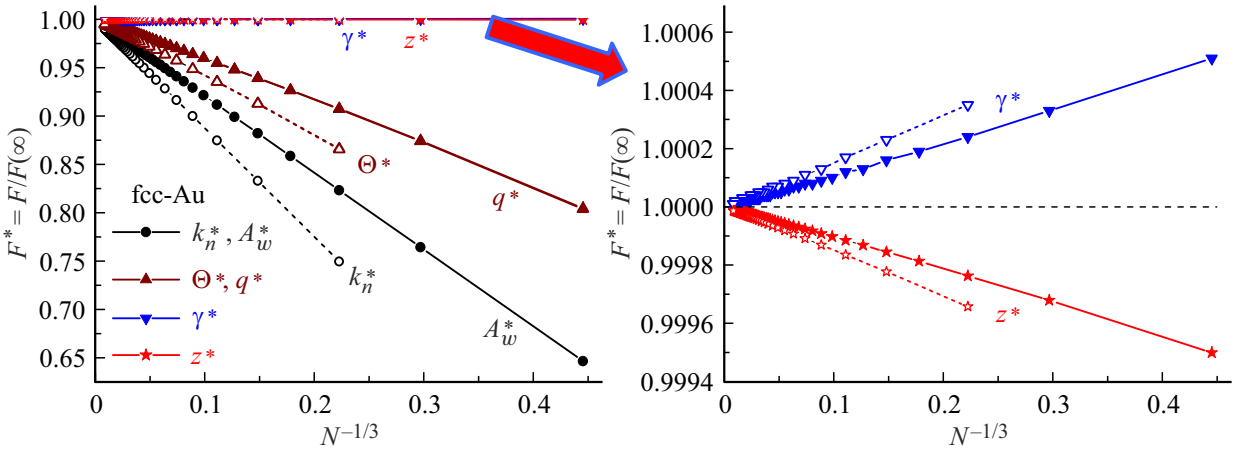

Figure 8. Isochoric (at $R = 1$) dependences of normalized functions: k_n^*, A_w^*, Θ^*, γ^*, q^* and z^* from $1/N^{1/3}$. For cube shape (at $f = 1$) solid symbols were obtained, and for rod-like shape at $f = 8$ open symbols were obtained. On the right graph dependences for the first and third Grüneisen parameters are shown in high zoom.

and experimental papers of other authors (for example, in [43,44,47,71,75–79]). At the same time in some papers (see summary in [11]) were observed the increase in elastic modulus B_T during the nanocrystal size decreasing. It was shown in Ref. [11] that this is associated with methods used in these papers for experimental or theoretical study of nanocrystals.

For example, in Ref. [80] by Raman spectrum study were detected the elastic modulus increasing of nano-diamond when its size increases. However, this was due to Hall–Petch effect for sample of pressed 2–5 nm diamond particles obtained by detonation method. Besides, $B_T(N)$ increasing can be attributed to the fact that nanopowder of diamond before pressing was additionally mechanically activated in a planetary ball mill. This resulted in significant change in surface properties of diamond nanogranules. Compression and mechanical activation of the diamond nanopowder resulted in B_T rise in near surface region of the nanocrystals. And as with nanocrystal size decreasing the contribution of the near-surface region increases, this resulted to increase in $B_T(N)$ — elastic modulus of the entire nanocrystal upon decrease in size of nano-diamond identified in Ref. [80]. This statement is also confirmed by the fact that diamond nanopowder prepared without compression and mechanical activation in Ref. [75] showed decrease in the elastic modulus with decrease in size of the diamond nanogranules.

For better understanding of effect of size and shape of nanocrystal on the thermal expansion coefficient and specific thermal capacity let's present the Helmholtz specific free energy of nanocrystal with Gibbs surface from Eq. (4) as sum of volume ($f_{\mathrm{H}_{in}}$) and surface contributions as follows:

$$f_{\mathrm{H}} = f_{\mathrm{H}_{in}} + \sigma\left(\frac{\Sigma}{N}\right).$$

If number of atoms in system is constant: $dN = 0$, then specific (per atom) entropy (s) and isochoric thermal capacity (c_v) of such system are determined by expressions of the following form [14,45,81]:

$$s = -\left(\frac{\partial f_{\mathrm{H}_{in}}}{\partial T}\right)_{v,N} - \left[\frac{\partial(\sigma\Sigma/N)}{\partial T}\right]_{v,N}$$

$$= s_{in} - \left[\left(\frac{\Sigma}{N}\right)\left(\frac{\partial\sigma}{\partial T}\right)_{v,N} + \sigma\left(\frac{\partial(\Sigma/N)}{\partial T}\right)_{v,N}\right],$$

$$c_v = T\left(\frac{\partial s}{\partial T}\right)_{v,N} = c_{v_{in}} - T\left\{\left(\frac{\Sigma}{N}\right)\left(\frac{\partial^2\sigma}{\partial T^2}\right)_{v,N}\right.$$

$$\left. + 2\left(\frac{\partial(\Sigma/N)}{\partial T}\right)_{v,N}\left(\frac{\partial\sigma}{\partial T}\right)_{v,N} + \sigma\left(\frac{\partial^2(\Sigma/N)}{\partial T^2}\right)_{v,N}\right\}. \quad (36)$$

If the specific surface Σ/N does not change with temperature at constant values of v and N, then for functions s and c_v from (36), and also for product $\alpha_p B_T$ we will obtain the expressions:

$$s = s_{in} - \left(\frac{\Sigma}{N}\right)\left(\frac{\partial\sigma}{\partial T}\right)_{v,N}, \quad c_v = c_{v_{in}} - \left(\frac{\Sigma}{N}\right)T\left(\frac{\partial^2\sigma}{\partial T^2}\right)_{v,N}, \quad (37)$$

$$\alpha_p B_T = \left(\frac{\partial s}{\partial v}\right)_T = (\alpha_p B_T)_{in}$$

$$- \left\{\left(\frac{\partial\sigma}{\partial T}\right)_{v,N}\left[\frac{\partial(\Sigma/N)}{\partial v}\right]_{T,N} + \left(\frac{\Sigma}{N}\right)\left[\frac{\partial(\partial\sigma/\partial T)_{v,N}}{\partial v}\right]_{T,N}\right\}. \quad (38)$$

As it was shown within RP-model [14,45,81], for specific values of volume, surface area and isochoric derivative of specific surface energy with respect to temperature we can obtain expressions:

$$v = \alpha c^3,$$

$$\Sigma/N = 6c^2\alpha_s(\alpha^2/N)^{1/3}Z_s(f)$$

$$= 6\alpha_s c^2(1 - k_n^*) = 6v^{2/3}(1 - k_n^*),$$

$$\left(\frac{\partial\sigma}{\partial T}\right)_{v,N} = -\left(\frac{\sigma'_\infty}{k_n^*}\right)F_E(y) < 0, \tag{39}$$

$$\sigma'_\infty = -\lim_{\substack{T\to\infty\\N\to\infty}}\left(\frac{\partial\sigma}{\partial T}\right)_{v,N} \cong \frac{k_\mathrm{B}}{4\alpha_s c^2}$$

$$= \frac{k_\mathrm{B}}{4v^{2/3}} = \frac{3k_\mathrm{B}}{2}\left(\frac{1-k_n^*}{\Sigma/N}\right). \tag{40}$$

Then from (39) and (40) we get the expressions:

$$T\left(\frac{\partial^2\sigma}{\partial T^2}\right)_{v,N} = -\left[\frac{\sigma'_\infty}{k_n^*(N,f)}\right]G_E(y),$$

$$\left[\frac{\partial(\partial\sigma)/\partial T)_{v,N}}{\partial v}\right]_{T,N} = \left(\frac{\sigma'_\infty}{vk_n^*}\right)\left[\frac{2}{3}F_E(y) - \gamma G_E(y)\right], \tag{41}$$

where function is introduced:

$$G_E(y) = -y\left[\frac{\partial F_E(y)}{\partial y}\right] = F_E(y)\left\{y\left[\frac{\exp(y)+1}{\exp(y)-1}\right] - 2\right\} \geq 0. \tag{42}$$

Using (39)–(42), Eqs. (37) and (38) can be converted to form:

$$s = s_{in} - \left(\frac{\Sigma}{N}\right)\left(\frac{\partial\sigma}{\partial T}\right)_{v,N} = s_{in} + \left(\frac{\Sigma}{N}\right)\left(\frac{\sigma'_\infty}{k_n^*}\right)F_E(y)$$

$$= s_{in} + \frac{3k_\mathrm{B}}{2}\left(\frac{1-k_n^*}{k_n^*}\right)F_E(y), \tag{43}$$

$$c_v = c_{v_{in}} - \frac{\Sigma}{N}T\left(\frac{\partial^2\sigma}{\partial T^2}\right)_{v,N} = c_{v_{in}} + \frac{3k_\mathrm{B}}{2}\left(\frac{1-k_n^*}{k_n^*}\right)G_E(y), \tag{44}$$

$$\alpha_p B_T = (\alpha_p B_T)_{in} + \frac{3k_\mathrm{B}}{2v}\gamma\left(\frac{1-k_n^*}{k_n^*}\right)G_E(y), \tag{45}$$

In „thermodynamic limit“ (i.e. when $N\to\infty$ and $V\to\infty$ at $v = V/N = \mathrm{const}$) from (11) we obtain $k_n^*(N\to\infty)\to 1$. Then surface contributions in Eqs. (43)–(45) disappear. We see from (39) and (41) that at $T = 0\,\mathrm{K}$ they satisfy the conditions (24), i.e. the third law of thermodynamics is satisfied at any size of nanocrystal.

Figure 9 shows the dependence of functions $E_w(y)$ and $F_E(y)$ from (7), and $G_E(y)$ from (42) on normalized temperature $1/y = T/\Theta_\mathrm{E}(N,f)$. As can be seen from (42) and Figure 9 that function $G_E(y)$ satisfies the conditions: $G_E(1/y=0)=0$, $G_E(1/y=\infty)=0$, and at $1/y = T/\Theta_\mathrm{E}(N,f) = 0.286$ reaches maximum: $\mathrm{MAX}[G_E(y)] = 0.676$. The following conclusions may be drawn from these results:

1) At $T = 0\,\mathrm{K}$ surface contributions to the specific entropy, thermal capacity, to product of $\alpha_p B_T$ and to thermal expansion coefficient disappear, not violating the third law of thermodynamics.

2) At $T/\Theta_\mathrm{E} = \infty$ surface contributions in specific isochoric thermal capacity from (44) and to product of $\alpha_p B_T$ from (45) disappear, not violating the law of classic statistical physics on equidistribution of kinetic energy among the degrees of freedom of the system, the consequence of which is the Dulong–Petit law.

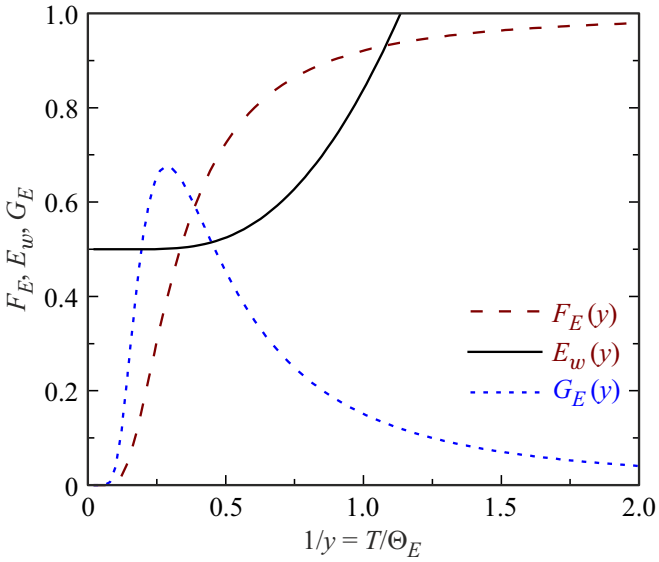

Figure 9. Functions $E_w(y)$, $F_E(y)$ and $G_E(y)$ vs. argument $1/y = T/\Theta_\mathrm{E}(N,f)$.

3) At $T_{\max}(N,f) = 0.2145\cdot\Theta(N,f)$ surface contributions in specific thermal capacity from (44) and in product of $\alpha_p B_T$ from (45) reach maximum.

4) During isomorphic-isothermal-isobaric decrease in nanocrystal size the maximum increases, and $T_{\max}$ decreases.

5) During isomorphic-isomeric-isothermal compression of nanocrystal the values of Θ and $T_{\max}$ increase.

Note that maximum of function $\Delta c_v(T) = c_v(T)_{\mathrm{Nano}} - c_v(T)_{\mathrm{Macro}}$ at low temperatures and $P = 0$ is identified also in papers of other authors (for example, in [82–87]). Maximum presence in function $\Delta\alpha_p(T) = \alpha_p(T)_{\mathrm{Nano}} - \alpha_p(T)_{\mathrm{Macro}}$ at low temperatures and $P = 0$ leads to increase in function $\alpha_p(T)_{\mathrm{Nano}}$ in range of low temperatures, see Figure 3. That's why if macrocrystal at low temperatures has negative thermal expansion coefficient (diamond, silicon etc.), the crystal transformation into nanoscale state can ensure isothermal increase in $\alpha_p(T \ll \Theta)$, up to positive value, as it was specified in Refs. [14,81].

We see from (43)–(45), that surface contributions in entropy, thermal capacity and in thermal expansion coefficient are positive. However, thermal variation of surface shape of the nanocrystal can provide definite contribution into both entropy, and thermal capacity of nanocrystal. If during isochoric heating the function Σ/N changes, then from (36) we see that additional (as compared to (37)) terms can result in some effects determined by only thermal variation of nanocrystal shape. If in formula for entropy in (36) the inequality

is met:

$$\left(\frac{\partial \ln(\Sigma/N)}{\partial T}\right)_{v,N} = \\ = \left(\frac{\partial \ln(Z_S(f))}{\partial T}\right)_{v,N} > -\left(\frac{\partial \ln(\sigma)}{\partial T}\right)_{v,N} > 0, \quad (46)$$

i. e. if specific surface during constant-volume heating increases greater then surface energy decreases, then surface contribution in the specific entropy of nanocrystal will be negative: $s_{sf} = s - s_{in} < 0$.

If in Eq. (36) for thermal capacity the condition is met:

$$\left(\frac{\Sigma}{N}\right)\left(\frac{\partial^2\sigma}{\partial T^2}\right)_{v,N} + 2\left(\frac{\partial(\Sigma/N)}{\partial T}\right)_{v,N}\left(\frac{\partial\sigma}{\partial T}\right)_{v,N} \\ + \sigma\left(\frac{\partial^2(\Sigma/N)}{\partial T^2}\right)_{v,N} > 0, \quad (47)$$

then surface contribution into the specific thermal capacity of nanocrystal will be negative: $c_{vsf} = c_v - c_{vin} < 0$. Such situation is possible for the nanocrystal with nonequilibrium morphology. For example, if during heating of „noncubic" (plate, rod-like or „fractal") nanocrystal its shape will go to energy optimal shape, and its specific surface area will decrease (at constant values of v and N), then the released in such way surface energy will decrease the specific thermal capacity of the nanocrystal. However, such relaxation processes shall not lead to breaching of the stability condition of thermodynamic equilibrium of the system [15]: $c_v > 0$ and $c_p > 0$. That's why, the realization of state with negative thermal capacity in the nanocrystal is impossible, as it was indicated in the Ref. [88].

The specific surface energy decreasing during isothermal decrease in the nanocrystal size was stated in many papers (see for example, [7,9,40,49,56]). From Eq. (13) we see that function $\sigma(N)$ decreasing during isomorphic-isobaric-isothermal decrease in N is due to both c/r_o increasing, and function $\Theta(k_n, c)$ decreasing. At the same time there are papers, where function $\sigma(N)$ increasing was obtained during isomorphic-isothermal decrease in N (for example see [8]). We showed in Refs. [10,32], that nanocrystal was compressed by surface pressure, which increases upon isomorphic-isothermal decrease in N. Such compression resulted in these calculations to rise in function $\sigma(N)$ during isomorphic-isothermal decrease in nanocrystal size.

It was shown in Ref. [11], that functions $B_T(N)$ and $\sigma(N)$ decreasing during isomorphic-isobaric-isothermal decrease in N results in increase in Poisson's ratio $\mu_p(N)$. At that the normalized (to value for macrocrystal) dependence for elastic modulus (B^*), Young's modulus (Y^*) and shear modulus (G^*) comply with the inequality:

$$B^* > Y^* > G^* > k_n^*. \quad (48)$$

The Poisson's ratio increasing upon thickness decreasing of nanoplate or nanorod was obtained both experimentally for diamond in [75] and gold in [89], and theoretically for W in [90], and for Cu and Ta in [91]. All these results confirm the correctness of our calculation method for functions $\sigma(T, v, N)$ and $P(T, v, N)$, that are basis of both temperature, and baric changes of all lattice properties of nanocrystal.

Note that for calculation of lattice and surface properties of single-component crystals we used model of Einstein crystal, i. e. model of independent harmonic oscillators. At that, see Eqs. [19,32,60,62], we obtained good agreement with experiment. This means that anharmonicity of atoms oscillations makes small contribution both into thermal expansion coefficient, and thermal capacity, and into surface properties and melting point of the crystal. This statement is in agreement with results of papers [54,59,92–96], in which show that effect of anharmonicity of atoms oscillation on properties of both classic [54,59,92–94], and quantum [59,95,96] single-component crystals is insignificant. We showed that melting is due to delocalization of definite portion of atoms of both macro- [61], and nanocrystal [31,97].

Also note that in the Eqs. (4)−(20), also as in our papers [10–14,16,19,32], the contribution of electronic subsystem into the thermodynamic parameters is not considered. This is due to the fact that potential (1), by definition, describes the pair interaction of electrically neutral atoms. In addition, as was shown in Refs. [98–101], the errors that arise in the lattice properties calculation due to the exclusion of the electronic subsystem from consideration are negligibly small. For example, as indicated in [98], for gold macrocrystal the contribution of the electronic subsystem to the pressure is 0.01 and 0.5 GPa at 1000 K and 5000 K, respectively. This contribution is much smaller than the error in pressure measurements at these temperatures.

5. Conclusion

Thus, by analytical method, that uses Mie−Lennard-Jones pair 4-parameter potential of interatomic interaction, the changes in equation of state and baric dependences of various properties of gold were studied during transition from macrocrystal to nanocrystal of cube or rod-like shape comprising $N = 306$ atoms.

It is shown that at $P = 0$ the specific (per atom) volume for nanocrystal is larger than in macrocrystal. At that the difference is larger the higher temperature is or the more nanocrystal shape deviates from the energy optimum one (cube for the RP model).

At any pressure and temperature during isothermal-isobaric decrease in N the following functions decrease: Θ, q, B_T, T_m. At that values of following properties increase: $\Theta'(P)$, γ, α_p, $|\alpha'_p(P)|$, $C_i(P)$, $|C'_i(P)|$, $|\sigma'(T)_i|$. It is shown that such properties as: $\alpha_p \cdot B_T$, $B'(P)$, σ, $\sigma'(P)$, $T'_m(P)$, can change their size dependence if $P-T$-conditions change.

It is shown that at any pressure the melting point $T_m(P, N, f)$ decreases both with isomorphic-isobaric de-

crease in the number of atoms N and with isomer-isobaric deviation of the nanocrystal shape from the energy optimal shape (for RP-models it is cube). It is shown that the value of the baric derivative of the melting point $T_m'(P)$ for nanocrystal at low pressures is greater, and at high pressures it is less than the value $T_m'(P)$ for a macrocrystal. In this case, the dependence of the function $T_m'(P)$ on the size of the nanocrystal is insignificant, i. e., for constant $N-f$-arguments the baric dependences $T_m(P, \infty)$ and $T_m(P, N, f)$ are practically parallel.

It is shown that during isothermal-isobaric decrease in N functions k_n, Θ and $\sigma(N)$ decrease more noticeable the larger the nanocrystal shape deviates from most energy optimal shape. This results in that upon the nanocrystal shape deviation from the energy optimal shape the size changes of baric dependences of nanocrystal properties increase.

Acknowledgments

The author would like to thank prof. V.M. Samsonov, and S.P. Kramynin, K.N. Magomedov, N.Sh. Gazanova, Z.M. Surkhayeva and M.M. Gadzhieva for fruitful discussions and assistance in study.

Conflict of interest

The author declares that he has no conflict of interest.

References

[1] N.R.C. Corsini, W.R. Little, A. Karatutlu, Y. Zhang, O. Ersoy, P.D. Haynes, C. Molteni, N.D.M. Hine, I. Hernandez, J. Gonzalez, F. Rodriguez, V.V. Brazhkin, A. Sapelkin. Nano Lett. **15**, *11*, 7334 (2015). DOI: 0.1021/acs.nanolett.5b02627
[2] F. Bai, K. Bian, X. Huang, Z. Wang, H. Fan. Chem. Rev. **119**, *12*, 7673 (2019). DOI: 10.1021/acs.chemrev.9b00023
[3] I.M. Padilla Espinosa, T.D.B. Jacobs, A. Martini. Nanoscale Res. Lett. **17**, *1*, 96 (2022). DOI: 10.1186/s11671-022-03734-z
[4] W.R. Tyson, W.A. Miller. Surf. Sci. **62**, *1*, 267 (1977). DOI: 10.1016/0039-6028(77)90442-3
[5] S.N. Zhevnenko, I.S. Petrov, D. Scheiber, V.I. Razumovskiy. Acta Materialia **205**, 116565 (2021). DOI: 10.1016/j.actamat.2020.116565
[6] S. Zhu, K. Xie, Q. Lin, R. Cao. Advances. Colloid. Interface Sci. **315**, 102905 (2023). DOI: 10.1016/j.cis.2023.102905
[7] X. Zhang, W. Li, H. Kou, J. Shao, Y. Deng, X. Zhang, J. Ma, Y. Li, X. Zhang. J. App. Phys. **125**, *18*, 185105 (2019). DOI: 10.1063/1.5090301
[8] H. Amara, J. Nelayah, J. Creuze, A. Chmielewski, D. Alloyeau, C. Ricolleau, B. Legrand. Phys. Rev. B **105**, *16*, 165403 (2022). DOI: 10.1103/PhysRevB.105.165403
[9] E.H. Abdul-Hafidh. J. Nanoparticle Res. **24**, *12*, 266 (2022). DOI: 10.1007/s11051-022-05638-6
[10] M.N. Magomedov. Phys. Rev. B **109**, *3*, 035405 (2024). DOI: 10.1103/PhysRevB.109.035405
[11] M.N. Magomedov. Phys. Solid State **62**, *12*, 2280 (2020). DOI: 10.1134/S1063783420120197
[12] M.N. Magomedov. Tech. Phys. **58**, *9*, 1297 (2013). DOI: 10.1134/S106378421309020X
[13] M.N. Magomedov. Phys. Solid State **46**, *5*, 954 (2004). DOI: 10.1134/1.1744976
[14] M.N. Magomedov. Crystallogr. Reps **62**, *3*, 480 (2017). DOI: 10.1134/S1063774517030142
[15] L.A. Girifalco, Statistical Physics of Materials, J. Wiley and Sons Ltd., New York (1973). 346 p.
[16] M.N. Magomedov. Phys. Solid State **63**, *10*, 1465 (2021). DOI: 10.1134/S1063783421090250.
[17] P. Richard, A. Castellano, R. Béjaud, L. Baguet, J. Bouchet, G. Geneste, F. Bottin. Phys. Rev. Lett. **131**, *20*, 206101 (2023). DOI: 10.1103/PhysRevLett.131.206101
[18] D.E. Fratanduono, M. Millot, D.G. Braun, S.J. Ali, A. Fernandez-Pañella, C.T. Seagle, J.-P. Davis, J.L. Brown, Y. Akahama, R.G. Kraus, M.C. Marshall, R.F. Smith, E.F. O'Bannon III, J.M. Mcnaney, J.H. Eggert. Science **372**, *6546*, 1063 (2021). DOI: 10.1126/science.abh0364
[19] M.N. Magomedov. Phys. Solid State **64**, *7*, 765 (2022). DOI: 10.21883/PSS.2022.07.54579.319
[20] G. Weck, V. Recoules, J.A. Queyroux, F. Datchi, J. Bouchet, S. Ninet, G. Garbarino, M. Mezouar, P. Loubeyre. Phys. Rev. B **101**, *1*, 014106 (2020). DOI: 10.1103/PhysRevB.101.014106.
[21] P. Cheyssac, R. Kofman, R. Garrigos. Phys. Scripta **38**, *2*, 164 (1988). DOI: 10.1088/0031-8949/38/2/009
[22] R. Garrigos, P. Cheyssac, R. Kofman. Z. Phys. D **12**, *1–4*, 497 (1989). DOI: 10.1007/BF01427006
[23] S.L. Lai, J.Y. Guo, V. Petrova, G. Ramanath, L.H. Allen. Phys. Rev. Lett. **77**, *1*, 99 (1996). DOI: 10.1103/PhysRevLett.77.99
[24] G. Kellermann, A.F. Craievich. Phys. Rev. B **78**, *5*, 054106 (2008). DOI: 10.1103/physrevb.78.054106
[25] F. Ercolessi, W. Andreoni, E. Tosatti. Phys. Rev. Lett. **66**, *7*, 911 (1991). DOI: 10.1103/physrevlett.66.911
[26] Y. Qi, T. Çağin, W.L. Johnson, W.A. Goddard III. J. Chem. Phys. **115**, *1*, 385 (2001). DOI: 10.1063/1.1373664
[27] T.S. Zhu, M. Li. Mater. Res. Bull. **63**, 253 (2015). DOI: 10.1016/j.materresbull.2014.12.010
[28] M.N. Magomedov. Tech. Phys. **56**, *9*, 1277 (2011). DOI: 10.1134/S106378421109012X
[29] M.N. Magomedov. Tech. Phys. **59**, *5*, 675 (2014). DOI: 10.1134/S1063784214050211
[30] M.N. Magomedov. Tech. Phys. **61**, *5*, 730 (2016). DOI: 10.1134/S1063784216050157
[31] M.N. Magomedov. J. Mol. Liq. **285**, 106 (2019). DOI: 10.1016/j.molliq.2019.04.032
[32] M.N. Magomedov. Phys. Solid State **66**, *3*, 428 (2024). DOI: 10.61011/PSS.2024.03.57947.272
[33] P.I. Dorogokupets, T.S. Sokolova, B.S. Danilov, K.D. Litasov. Geodynamicsn & Tectonophysics **3**, *2*, 129 (2012). DOI: 10.5800/GT-2012-3-2-0067
[34] E.N. Ahmedov. J. Phys.: Conf. Ser. **1348**, *012002*, 1 (2019). DOI: 10.1088/1742-6596/1348/1/012002
[35] S.P. Kramynin. Phys. Met. Metallography **123**, *2*, 107 (2022). DOI: 10.1134/S0031918X22020065
[36] S.P. Kramynin. J. Phys. Chem. Solids **152**, 109964 (2021). DOI: 10.1016/j.jpcs.2021.109964
[37] S.P. Kramynin. Solid State Sci. **124**, 106814 (2022). DOI: 10.1016/j.solidstatesciences.2022.106814
[38] I.F. Golovnev, E.I. Golovneva. Phys. Mesomech. **23**, *3*, 189 (2020). DOI: 10.1134/S1029959920030017

[39] M. Zhao, Y. Xia. Nature Rev. Mater. **5**, *6*, 440 (2020). DOI: 10.1038/s41578-020-0183-3
[40] S. Xiong, W. Qi, Y. Cheng, B. Huang, M. Wang, Y. Li. Phys. Chem. Chem.Phys. **13**, *22*, 10652 (2011). DOI: 10.1039/c0cp90161j
[41] M. Zhu, J. Liu, Q. Huang, J. Dong, X. Yang. J. Phys. D **55**, *48*, 485303 (2022). DOI: 10.1088/1361-6463/ac9485
[42] E. Purushotham, V. Radhika. Mater. Today: Proc. **47**, *15*, 4993 (2021). DOI: 10.1016/j.matpr.2021.04.451
[43] C.Q. Sun. Progress. Mater. Sci. **54**, *2*, 179 (2009). DOI: 10.1016/j.pmatsci.2008.08.001
[44] M. Goyal, B.R.K. Gupta. Mod. Phys. Lett. B **33**, *26*, 1950310 (2019). DOI: 10.1142/s021798491950310x
[45] M.N. Magomedov. J. Surf. Investigation. X-ray, Synchrotron. Neutron Techniques **6**, *1*, 86 (2012). DOI: 10.1134/S1027451012010132
[46] Y.F. Zhu, J.S. Lian, Q. Jiang. J. Phys. Chem. C **113**, *39*, 16896 (2009). DOI: 10.1021/jp902097f
[47] V. Pandey, M. Kumar. Pramana **97**, *3*, 88 (2023). DOI: 10.1007/s12043-023-02552-x
[48] G. Kellermann, F.L.C. Pereira, A.F. Craievich. J. Non-Cryst. Solids **635**, 122995 (2024). DOI: 10.1016/j.jnoncrysol.2024.122995
[49] D. Shekhawat, M. Vauth, J. Pezoldt. Inorganics **10**, *4*, 56 (2022). DOI: 10.3390/inorganics10040056
[50] S. Schönecker, X. Li, B. Johansson, S.K. Kwon, L. Vitos. Sci. Rep. **5**, *1*, 14860 (2015). DOI: 10.1038/srep14860
[51] T. Cheng, D. Fang, Y. Yang. App. Surf. Sci. **393**, 364 (2017). DOI: 10.1016/j.apsusc.2016.09.147
[52] D. Scheiber, O. Renk, M. Popov, L. Romaner. Phys. Rev. B **101**, *17*, 174103 (2020). DOI: 10.1103/PhysRevB.101.174103
[53] A.O. Tipeev, J.P. Rino, E.D. Zanotto. J. Chem. Phys. **155**, *9*, 094101 (2021). DOI: 10.1063/5.0059882
[54] A. Forslund, A. Ruban. Phys. Rev. B **105**, *4*, 045403 (2022). DOI: 10.1103/PhysRevB.105.045403
[55] C. Li, S. Lu, S. Divinski, L. Vitos. Acta Mater. **255**, 119074 (2023). DOI: 10.1016/j.actamat.2023.119074
[56] V.M. Samsonov, S.A. Vasilev, I.V. Talyzin, K.K. Nebyvalova, V.V. Puitov. Russ. J. Phys. Chem. A **97**, *8*, 1751 (2023). DOI: 10.1134/S003602442308023X
[57] G. Kellermann, F.L.C. Pereira, A.F. Craievich. J. Appl. Cryst. **53**, *2*, 455 (2020). DOI: 10.1107/S1600576720002101
[58] L. Keerthana, G. Dharmalingam. J. Phys. Chem. Solids **185**, 111800 (2024). DOI: 10.1016/j.jpcs.2023.111800
[59] G. de With. Chem. Rev. **123**, *23*, 13713 (2023). DOI: 10.1021/acs.chemrev.3c00489
[60] M.N. Magomedov. Phys. Solid State **65**, *5*, 708−717 (2023). DOI: 10.21883/PSS.2023.05.56040.46
[61] M.N. Magomedov. Phys. Met. Metallography **105**, *2*, 116 (2008). DOI: 10.1134/S0031918X08020038
[62] M.N. Magomedov. Phys. Solid State **66**, *2*, 221 (2024). DOI: 10.61011/PSS.2024.02.57919.241
[63] D. Errandonea. J. Appl. Phys. **108**, *3*, 033517 (2010). DOI: 10.1063/1.3468149
[64] D.M. Foster, T. Pavloudis, J. Kioseoglou, R.E. Palmer. Nature Commun. **10**, *1*, 2583 (2019). DOI: 10.1038/s41467-019-10713-z
[65] J. Chen, X. Fan, J. Liu, C. Gu, Y. Shi, D.J. Singh, W. Zheng. J. Phys. Chem. C **124**, *13*, 7414 (2020). DOI: 10.1021/acs.jpcc.9b10769
[66] C. Zeni, K. Rossi, T. Pavloudis, J. Kioseoglou, S. de Gironcoli, R.E. Palmer, F. Baletto. Nature Commun. **12**, *1*, 6056 (2021). DOI: 10.1038/s41467-021-26199-7
[67] B.K. Pandey, R.L. Jaiswal. Physica B: Condensed Matter **651**, 414602 (2023). DOI: 10.1016/j.physb.2022.414602
[68] H. Sheng, B. Xiao, X. Jiang. Physica B: Condens. Matter **667**, 415193 (2023). DOI: 10.1016/j.physb.2023.415193
[69] G. Poletaev, A. Sannikov, Y. Bebikhov, A. Semenov. Mol. Simul. **50**, *10*, 1 (2024). DOI: 10.1080/08927022.2024.2342972
[70] E.N. Ahmedov. Physica B: Condens. Matter **571**, 252 (2019). DOI: 10.1016/j.physb.2019.07.027
[71] B.S. Murty, M.K. Datta, S.K. Pabi. Sādhanā **28**, *1−2*, 23 (2003). DOI: 10.1007/BF02717124
[72] M.S. Omar. Int. J. Thermophys. **37**, *1*, 11 (2016). DOI: 10.1007/s10765-015-2026-9
[73] Y.H. Zhao, Y.T. Zhu. Rev. Adv. Mater. Sci. **48**, *1*, 52 (2017). https://www.ipme.ru/e-journals/RAMS/no_14817/04_14817_zhao.pdf
[74] M.S. Omar. J. Therm. Anal. Calorim. **148**, *24*, 14023 (2023). DOI: 10.1007/s10973-023-12689-x
[75] M. Mohr, A. Caron, P. Herbeck-Engel, R. Bennewitz, P. Gluche, K. Brühne, H.-J. Fecht. J. Appl. Phys. **116**, *12*, 124308 (2014). DOI: 10.1063/1.4896729
[76] W. Li, X. Wang, L. Gao, Y. Lu, W. Wang. Materials **12**, *23*, 3913 (2019). DOI: 10.3390/ma12233913
[77] J.J. Li, B.B. Lu, H.J. Zhou, C.Y. Tian, Y.H. Xian, G.M. Hu, R. Xia. Phys. Lett. A **383**, *16*, 1922 (2019). DOI: 10.1016/j.physleta.2018.10.053
[78] X. Ou, Y. Shen, Y. Yang, Z. You, P. Wang, Y. Yang, X. Tian. Materials **16**, *13*, 4618 (2023). DOI: 10.3390/ma16134618
[79] Y.Q. Hu, J.F. Xu, L. Su, Y.H. Zhang, S.H. Ding, Y.H. Shen, R. Xia. Mater. Chem. Phys. **296**, 127270 (2023). DOI: 10.1016/j.matchemphys.2022.127270
[80] M. Popov, V. Churkin, D. Ovsyannikov, A. Khabibrakhmanov, A. Kirichenko, E. Skryleva, Y. Parkhomenko, M. Kuznetsov, S. Nosukhin, P. Sorokin, S. Terentiev, V. Blank. Diam. Relat. Mater. **96**, 52 (2019). DOI: 10.1016/j.diamond.2019.04.033
[81] M.N. Magomedov. J. Surface Investigation. X-ray, Synchrotron Neutron Techn. **9**, *6*, 1236 (2015). DOI: 10.1134/S1027451015060154
[82] V.N. Likhachev, G.A. Vinogradov, M.I. Alymov. Phys. Lett. A **357**, *3*, 236 (2006). DOI: 10.1016/j.physleta.2006.04.050
[83] I. Avramov, M. Michailov. J. Phys.: Condens. Matter **20**, *29*, 295224 (2008). DOI: 10.1088/0953-8984/20/29/295224
[84] H. Lei, J. Li, J. Luo. Nanoscale **7**, *15*, 6762 (2015). DOI: 10.1039/C5NR00056D
[85] R. Carles, P. Benzo, B. Pécassou, C. Bonafos. Sci. Rep. **6**, *1*, 39164 (2016). DOI: 10.1038/srep39164
[86] T. Vasina, J. Bernard, Magali Benoit, F. Calvo. Phys. Rev. B **105**, *24*, 245406 (2022). DOI: 10.1103/PhysRevB.105.245406
[87] K. Gu, H. Wu, J. Su, P. Sun, P.H. Tan, H. Zhong. Nano Lett. **24**, *13*, 4038 (2024). DOI: 10.1021/acs.nanolett.4c01021
[88] K. Michaelian, I. Santamaría-Holek. Entropy **19**, *7*, 314 (2017). DOI: 10.3390/e19070314
[89] A.I. Oliva, G.G. Comparán-Rodriguez, V. Sosa, A.I. Oliva-Avilés. J. Mater. Sci. **58**, *20*, 8563 (2023). DOI: 10.1007/s10853-023-08536-x
[90] P. Villain, P. Beauchamp, K.F. Badawi, P. Goudeau, P.-O. Renault. Scr. Mater. **50**, *9*, 1247 (2004). DOI: 10.1016/j.scriptamat.2004.01.033

[91] M. Krief, Y. Ashkenazy. Phys. Rev. Res. **6**, *2*, 023253 (2024). DOI: 10.1103/PhysRevResearch.6.023253
[92] B. Grabowski, L. Ismer, T. Hickel, J. Neugebauer. Phys. Rev. B **79**, *13*, 134106 (2009). DOI: 10.1103/PhysRevB.79.134106
[93] C. Freysoldt, B. Grabowski, T. Hickel, J. Neugebauer, G. Kresse, A. Janotti, C.G. Van de Walle. Rev. Mod. Phys. **86**, *1*, 253 (2014). DOI: 10.1103/RevModPhys.86.253
[94] D.D. Satikunvar, N.K. Bhatt, B.Y. Thakore. J. App. Phys. **129**, *3*, 035107 (2021). DOI: 10.1063/5.0022981
[95] M. Borinaga, I. Errea, M. Calandra, F. Mauri, A. Bergara. Phys. Rev. B **93**, *17*, 174308 (2016). DOI: 10.1103/PhysRevB.93.174308
[96] I. Loa, F. Landgren. J. Phys.: Condens. Matter **36**, *18*, 185401 (2024). DOI: 10.1088/1361-648X/ad1e08
[97] M.N. Magomedov. Tech. Phys. **55**, *9*, 1373 (2010). DOI: 10.1134/S1063784210090227
[98] M. Matsui. J. Phys.: Conf. Ser. — IOP Publ. **215**, *1*, 012197 (2010). DOI: 10.1088/1742-6596/215/1/012197
[99] X. Huang, F. Li, Q. Zhou, Y. Meng, K.D. Litasov, X. Wang, B. Liu, T. Cui. Sci. Rep. **6**, 19923 (2016). DOI: 10.1038/srep19923
[100] A.M. Molodets, A.A. Golyshev, D.V. Shakhrai. J. Exp. Theor. Phys. **124**, *3*, 469 (2017). DOI: 10.1134/S1063776117030049.
[101] D.K. Belashchenko. Physics. Uspekhi **63**, *12*, 1161 (2020). DOI: 10.3367/UFNe.2020.01.038761.

Translated by I.Mazurov